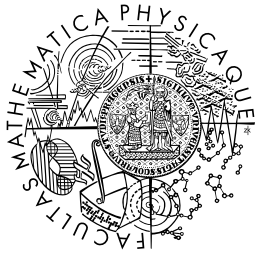

FACULTY
OF MATHEMATICS
AND PHYSICS
Charles University

MASTER THESIS

Bc. Dominik Starý

Leptogenesis in minimal grand unified models

Institute of Particle and Nuclear Physics

Supervisor of the master thesis: doc. Ing. Michal Malinský, Ph.D.
Study programme: Theoretical Physics
Study branch: FTFP

Prague 2024

I declare that I carried out this master thesis independently, and only with the cited sources, literature and other professional sources. It has not been used to obtain another or the same degree.

I understand that my work relates to the rights and obligations under the Act No. 121/2000 Sb., the Copyright Act, as amended, in particular the fact that the Charles University has the right to conclude a license agreement on the use of this work as a school work pursuant to Section 60 subsection 1 of the Copyright Act.

In ..... date ....

Author's signature

I would like to express my gratitude to everyone who helped me both professionally and mentally during the writing of my master thesis. First of all, I would like to thank my supervisor doc. Ing. Michal Malinský, Ph.D., for his kind and patient guidance and invaluable advice. I am also very grateful to Vasja Susič, Ph.D., for his expert advice and valuable insights on programming, and for providing me with the Mathematica package that implements the differential evolution algorithm. A special thanks to my colleague Hedvika Gedeon for collaborating on a shared part of the code that was used in my research and that she will use in her research. Last but not least, I would like to thank my family, friends, and my girlfriend for their unwavering patience and support.

Title: Leptogenesis in minimal grand unified models

Author: Bc. Dominik Starý

Institute: Institute of Particle and Nuclear Physics

Supervisor: doc. Ing. Michal Malinský, Ph.D., Institute of Particle and Nuclear Physics

Abstract: We investigate whether successful leptogenesis driven by heavy right-handed neutrino decays can be compatible with flavour fits within the minimal and potentially realistic non-supersymmetric SO(10)-based model with Yukawa sector composed of $\mathbf{10}_H$ and $\overline{\mathbf{126}}_H$, and with additionally imposed Peccei-Quinn symmetry. To this end, we solve density matrix equations and renormalization group equations for effectively direct symmetry breaking of SO(10) down to the Standard Model. We scan over the parameter space and generate a number of configurations compatible with flavour fits. One of the most striking results of this analysis is that we obtain configurations that give the value of the baryon asymmetry of the Universe within an order of magnitude of the measured value, despite the fitting procedure independent of the leptogenesis yield. Moreover, leptogenesis in this region of parameter space is predominantly driven by decays of the second lightest right-handed neutrino. Furthermore, the analysis shows that the fitted $B-L$ breaking scale is consistent with previous studies, despite not explicitly incorporating gauge coupling unification and full renormalization group equations with $B-L$ breaking. We also provide the best flavour fit for the model without additionally imposed Peccei-Quinn symmetry that shows preserving of characteristics and some predictions of the first model.

Keywords: baryogenesis, leptogenesis, matter-antimatter asymmetry, grand unification

Contents

Introduction

Since the discovery of the Higgs boson in 2012, the Standard Model (SM) has been regarded as a complete and realistic framework for describing particles and their interactions that is in excellent agreement with the outcomes of the vast majority of experimental observations.

However, despite its remarkable success, the SM as formulated by S. L. Glashow [1], S. Weinberg [2] and A. Salam [3] suffers from a fundamental flaw (leaving aside the fact that it does not involve gravity) – it describes neutrinos as massless particles, which is in direct contradiction with the experimental evidence of neutrino flavour oscillations from measurements by the Super-Kamiokande [4, 5] and KamLAND [6] collaborations. These results imply that at least two of the three neutrino states are massive, providing a clear signal of physics beyond the SM.

Another equally interesting, though rather cosmetic, shortcoming of the SM is its inability to provide a satisfactory answer to some of the most profound mysteries in modern cosmology, namely the particle nature of dark matter and the origin of the observed matter-antimatter asymmetry of the Universe (also known as the baryon asymmetry of the Universe, BAU). By the 'cosmetic shortcoming', we point to a certain loophole in the ΛCDM model.Despite extensive searches for dark matter particles that could explain its observed gravitational effects, no signals of their interaction have yet been detected. Regarding the BAU, although observations of the Cosmic Microwave Background (CMB) radiation [7] and the abundance of light elements produced in Big Bang Nucleosynthesis [8] provide compelling evidence that the asymmetry is significantly larger than what the SM can reproduce, this discrepancy could potentially be a matter of initial conditions. On the other hand, such a Universe would have to be precisely fine-tuned.

Remarkably, the simple extension of the SM in the form of adding three right-handed neutrinos (RHNs), i.e., the first thing that comes to mind in attempt to incorporate neutrino masses in the SM, resulting in the seesaw mechanism [9–12], also provides an interesting explanation of the BAU via the so-called leptogenesis [13] – a mechanism of dynamical generation of lepton asymmetry through CP-violating out-of-equilibrium (OOE) decays of these new particles in the hot early Universe. According to this scenario, the produced lepton asymmetry was subsequently partially converted into baryon asymmetry by non-perturbative sphaleron processes [13–17] – instanton-like processes that violate $B+L$, the sum of baryon and lepton numbers, and conserve $B-L$.

In fact, this extension is not the only way how to introduce neutrino masses and leptogenesis. At the tree level, one is also allowed to add a left-handed scalar triplet [11, 18–20], or a left-handed fermionic triplet [21, 22].

However, with any such extension, additional free parameters are introduced into the model.And the more free parameters a theory has, the less predictive it becomes, because it is more flexible to accommodate the observations. The SM itself contains 19 free parameters – 3 gauge couplings corresponding to the SM gauge group $\mathrm{SU}(3)_c \times \mathrm{SU}(2)_L \times \mathrm{U}(1)_Y$, 6 quark masses, 3 charged-lepton masses, 3 quark mixing angles, the quark CP phase, the Higgs boson mass, the Higgs vacuum expectation value, and the strong CP phase. For instance, in the

seesaw extension with three RHNs, another 18 parameters have to be added. These parametrize the neutrino Yukawa matrix, which is also crucial for the computation of the lepton asymmetry. One can express the neutrino Yukawa matrix in the Casas-Ibarra parametrization [23] in terms of observables, of which only 3 lepton mixing angles and the light neutrino mass squared differences have been determined from experiments so far. Consequently, the neutrino Yukawa matrix is largely undetermined.

Here, decades of research on Grand Unified Theories (GUTs) [24, 25] come in handy, since GUTs exhibit baryon and lepton number violation (BLNV) already at perturbative level, and greater predictability than the SM, typically manifested by additional constraints on the Yukawa couplings.

Both supersymmetric (SUSY) and non-SUSY GUT models have been thoroughly investigated – among the other things, their potential capabilities to accommodate the experimental measurements have been explored. Among the most promising models so far are those based on the gauge group SO(10), which has several attractive properties: it accommodates all fermions of a given generation, including RHNs, in a single 16-dimensional multiplet; it naturally provides the seesaw mechanism mediated by both RHNs and the left-handed scalar triplet; it restores left-right symmetry at high energies [11]; and it is anomaly-free.

Many previous studies have focused on flavour fits in different setups of SO(10) models. They have examined, e.g., the impact of specific symmetry-breaking chains and intermediate scales [26–28], normal and inverted neutrino mass hierarchies [28], types of seesaw mechanism [29], and different Yukawa sectors [28, 30].

In this work, we focus on non-SUSY renormalizable SO(10) models both without and with an additional global Peccei-Quinn symmetry [30–32], and with a minimal Yukawa sector containing a complexified scalar representation $\mathbf{10}_H$ and a complex scalar representation $\overline{\mathbf{126}}_H$. At the same time, we consider the field content extended by both RHNs and the left-handed scalar triplet.

The purpose of this thesis is to investigate the possibility of successful leptogenesis while maintaining consistent flavour fits within the framework of these models, thus building naturally upon previous works [33, 34].

This thesis is organized as follows. In Chapter 1, we introduce minimal extensions of the SM leading to seesaw mechanism types I and II. Chapter 2 provides a condensed review of the formalism of leptogenesis, including Boltzmann equations that govern its dynamics. In Chapter 3, we introduce the basic concepts of GUTs as an attractive framework for studying leptogenesis, with a particular focus on non-SUSY SO(10)-based models that we consider throughout this thesis. Chapter 4 details our methodological approach and numerical analysis – the fitting procedure, the implementation of the tools used to solve the Boltzmann equations (BEs) and renormalization group equations (RGEs), and the parameter space exploration. Last chapters presents and summarizes our main results, findings and conclusions, and outline some possible directions for future research. In Appendix B, one can find a list of used RGEs and conventions.

1. Origin of neutrino masses

1.1 Seesaw mechanism type I

In the SM, charged-fermion masses are generated via the famous Higgs mechanism [35, 36]. The interaction with the Higgs field is described by a Yukawa-type interaction whose structure involves an $\mathrm{SU}(2)_L$ left-handed doublet and a right-handed singlet, both of which represent the fermion fields. Since neutrinos in the SM lack their right-handed counterparts, they are inherently massless.

This observation suggests a remedy to address the non-zero neutrino masses in the form of a simple and intuitive extension: filling the vacancy in the lepton sector by adding three RHNs, i.e., one per generation, which are singlets under the SM gauge group. In addition, in this extension, neutrinos are commonly assumed to be Majorana, reflecting their electric neutrality. Despite its simplicity, however, such an extension leads to profound implications.

Let us denote the newly introduced fields by N_R. To incorporate them, we equip the SM Lagrangian with the following structure (adopting the convention from [37])

$$\mathcal{L}_{RHN} = i\overline{N_R}\partial\!\!\!/ N_R - Y_\nu \overline{N_R}\tilde{\Phi}^\dagger L_L - \frac{1}{2}\overline{N_R} M_R N_R^c + \text{h.c.}, \tag{1.1}$$

which consists of a kinetic term, a Yukawa interaction term, and a Majorana mass term, respectively. Here, Y_ν is a Dirac-type neutrino Yukawa matrix, $\tilde{\Phi} = i\sigma_2\Phi^*$ with $\Phi = (1, 2, +1/2)$ being the Higgs doublet, $L_L = (L_L^1, L_L^2, L_L^3)$ represents the $\mathrm{SU}(2)_L$ lepton doublets, and M_R is a complex symmetric Majorana mass matrix.

With the Lagrangian (1.1) at hand, one can proceed to find the neutrino mass eigenstates and eigenvalues. In the broken phase, the corresponding non-derivative part of (1.1) then yields a key formula that describes the mechanism by which the SM-like neutrinos acquire their small but non-zero masses in this setup. The formula for the mass matrix M_ν of physical active neutrinos is as follows

$$M_\nu = -v^2 Y_\nu^T M_R^{-1} Y_\nu \equiv M_\nu^I, \tag{1.2}$$

where $v = 246\,\text{GeV}/\sqrt{2} \doteq 174\,\text{GeV}$ is the vacuum expectation value (VEV) of the SM Higgs field. The reason for renaming M_ν to M_ν^I will become clear soon. Eq. (1.2) implies that for the SM-like neutrino masses to be in the sub-eV range (as indicated by the results of the tritium β decay experiment [38] or cosmological limits [39, 40]), the RHNs should be extremely heavy unless the Yukawa matrix Y_ν is suppressed. For instance, if $|Y_\nu| \sim 0.1$, the order of magnitude estimate for the Majorana mass gives $10^{11-12}\,\text{GeV}$. Due to the inverse proportionality of the SM-like neutrino masses to the large-scale masses of the RHNs, this mechanism is called the seesaw, or more precisely the type-I seesaw mechanism [9–12] (hence the superscript 'I' in Eq. (1.2)). 'Type I' refers to the fact that this is only one of the three canonical realisations of the seesaw mechanism. We will come to that in the next section. See also Appendix A.

At least two remarks are worth mentioning here. First, the introduced extension exhibits perturbative lepton number violation (LNV). Second, once the lepton sector is supplemented by three RHNs, a quark-like flavour structure is

recovered. This enables leptonic mixings and neutrino flavour oscillations [4–6]. The lepton-sector counterpart of the CKM matrix, connecting flavour eigenstates to mass eigenstates, is the so-called Pontecorvo-Maki-Nakagawa-Sakata (PMNS) matrix. This matrix – let us denote it by $V_{\rm PMNS}$ – is parametrised by three mixing angles, $\theta_{12}^{\rm PMNS}$, $\theta_{13}^{\rm PMNS}$, $\theta_{23}^{\rm PMNS}$, and three CP-violating phases, $\delta_{\rm CP}$, ϕ_1 and ϕ_2:

$$V_{\rm PMNS} = \begin{pmatrix} c_{12}c_{13} & s_{12}c_{13} & s_{13}e^{-i\delta_{\rm CP}} \\ -s_{12}c_{23} - c_{12}s_{23}s_{13}e^{i\delta_{\rm CP}} & c_{12}c_{23} - s_{12}s_{23}s_{13}e^{i\delta_{\rm CP}} & s_{23}c_{13} \\ s_{12}s_{23} - c_{12}c_{23}s_{13}e^{i\delta_{\rm CP}} & -c_{12}s_{23} - s_{12}c_{23}s_{13}e^{i\delta_{\rm CP}} & c_{23}c_{13} \end{pmatrix} \cdot \\ \cdot \operatorname{diag}\left(e^{-i\phi_1/2}, e^{-i\phi_2/2}, 1\right), \tag{1.3}$$

where $s_{ij} = \sin\theta_{ij}^{\rm PMNS}$ and $c_{ij} = \cos\theta_{ij}^{\rm PMNS}$.

1.2 Seesaw mechanism type II

The extension of the SM by RHNs is the first thing that comes to mind when trying to introduce neutrino masses. However, it is far from the only way. Another extension we will consider in our analysis is the addition of a massive scalar [11, 18] Δ_L transforming as (1,3,+1) under the SM gauge group $\mathrm{SU}(3)_c \times \mathrm{SU}(2)_L \times \mathrm{U}(1)_Y$,

$$\Delta_L = \begin{pmatrix} \frac{1}{\sqrt{2}}\Delta_L^+ & \Delta_L^{++} \\ \Delta_L^0 & -\frac{1}{\sqrt{2}}\Delta_L^+ \end{pmatrix}, \tag{1.4}$$

where Δ_L^0, Δ_L^+, and Δ_L^{++} are the components of the triplet. This extension is referred to as the type-II seesaw.

The relevant part of Lagrangian involving the triplet is given by [20]

$$\mathcal{L}_\Delta \ni -M_\Delta^2 \mathrm{Tr}\left(\Delta_L^\dagger \Delta_L\right) - Y_\Delta \overline{L_L^c} i\sigma_2 \Delta_L L_L + \mu \Phi^T i\sigma_2 \Delta_L \Phi + \mathrm{h.c.}, \tag{1.5}$$

where M_Δ is the mass of Δ_L and Y_Δ and μ are its couplings to the pair of lepton doublets and the pair of Higgs doublets, respectively.

The neutrino mass matrix generated by Δ_L is then given by

$$M_\nu^{II} = v_\Delta Y_\Delta \equiv M_L, \tag{1.6}$$

where v_Δ is an induced VEV that the neutral component of Δ_L acquires,

$$v_\Delta \equiv \langle \Delta_L^0 \rangle = \frac{\mu^* v^2}{M_\Delta^2}. \tag{1.7}$$

Thus, the light neutrino masses are again inversely proportional to the mass of the added particle.

The combination of both type-I and type-II seesaw extensions yields a combined seesaw formula:

$$M_\nu = M_\nu^{II} + M_\nu^I = M_L - v^2 Y_\nu^T M_R^{-1} Y_\nu. \tag{1.8}$$

The introduced seesaw extensions of the SM provides an elegant explanation for the smallness of neutrino masses. Nevertheless, this is not the end of the story, as the extension has interesting implications for a completely different phenomenon, which at first glance has nothing to do with its original purpose.

2. Leptogenesis

In the previous chapter, we presented a SM extension that exhibits lepton number violation. Let us now turn to another phenomenon that the SM cannot explain – the observed baryon asymmetry of the Universe, which, on the contrary, may be related to the baryon number violation. Surprisingly, it turns out that in the seesaw extension it is possible to generate a sufficiently high baryon asymmetry by means of a different mechanism – leptogenesis [13].

2.1 Baryon asymmetry of the Universe

In the present Universe, baryonic matter obviously dominates over rarely occurring antimatter (antibaryons). At first glance, this asymmetric distribution of matter and antimatter seems to contradict the reasonable assumption that the Universe evolved from a state with zero net baryon number.

The BAU may be quantified by a baryon-to-photon number density ratio η_B, which is defined as

$$\eta_B = \frac{n_B - n_{\bar{B}}}{n_\gamma}, \tag{2.1}$$

where n_B, $n_{\bar{B}}$, and n_γ are the number densities of baryons, anti-baryons, and photons, respectively, at present time. The ΛCDM model of the cosmic evolution suggests a way to measure this quantity, since the spectrum of the CMB radiation [7] is sensitive to the value of η_B. The latest results of the Planck collaboration [7] establish the following value of η_B based on CMB data

$$\eta_B^{\mathrm{CMB}} = (6.125 \pm 0.027) \times 10^{-10}. \tag{2.2}$$

However, this value is about ten orders of magnitude above the estimate, which one can obtain from the SM.

The conundrum lies in the following: if the current Universe is not a descendant of precisely fine-tuned asymmetric initial conditions[1], how did it evolve from a state, where matter and antimatter were created in equal amounts, to its current matter-dominated state? This calls for a mechanism of generating the asymmetry dynamically. Such a process is referred to as baryogenesis.

In order for baryogenesis to be possible, processes have to take place in the primordial plasma that fulfill three Sakharov's conditions [41]:

1. These processes violate baryon number.
2. They violate C and CP.
3. The Universe has to undergo out-of-thermal-equilibrium phase.

[1]Moreover, there is a well-founded suspicion that the early universe underwent a phase of inflation, which would have exponentially diluted any initial asymmetry.

2.2 Electroweak baryogenesis

Surprisingly, the SM contains all the necessary means for baryogenesis, including BNV processes (albeit only at the non-perturbative level) such as sphaleron processes [14] –instanton-like processes at finite temperature that violate $B + L$ and conserve $B - L$.

The SM thus offers the following picture of baryogenesis. If the electroweak phase transition (EWPT) was first-order, it would lead to the formation of expanding bubbles with broken phase inside, while outside the bubbles the phase would still be symmetric. As the bubbles would expand, the passing bubble walls would separate fermions due to CP-violating processes taking place in the plasma. However, sphaleron processes that are in thermal equilibrium above the EWPT [16] would wash out the asymmetry outside the bubbles. In contrast, inside the bubbles, they would be suppressed and the asymmetry would survive.

The mechanism just described is referred to as electroweak baryogenesis [17]. Unfortunately, the situation with the second and third Sakharov's conditions turns out to be problematic in the SM. CP-violating processes are screened in the hot and dense plasma [42], and regarding the EWPT, it was likely second-order (with respect to the measured value of the Higgs boson mass $m_H \approx 125\,\mathrm{GeV}$), not first-order as required.

2.3 Decays of right-handed neutrinos and a scalar triplet

Returning to the type-I and type-II seesaw extensions, with the new fields N_R's and Δ_L at hand, we can explore an alternative approach to baryogenesis. Namely, one may try to calculate the CP asymmetry of the decays of the i-th heavy neutrino mass eigenstate N_R^i or of the heavy scalar triplet Δ_L into leptons and antileptons, i.e.

$$\epsilon_{N_R^i} = \sum_\alpha \frac{\Gamma(N_R^i \to L^\alpha \Phi^*) - \Gamma(N_R^i \to \overline{L^\alpha}\Phi)}{\Gamma(N_R^i \to L^\alpha \Phi^*) + \Gamma(N_R^i \to \overline{L^\alpha}\Phi)} \tag{2.3}$$

in the case of the RHN decays, and similarly,

$$\epsilon_\Delta = 2\frac{\Gamma(\Delta_L^* \to LL) - \Gamma(\Delta_L \to \bar{L}\bar{L})}{\Gamma(\Delta_L^* \to LL) + \Gamma(\Delta_L \to \bar{L}\bar{L})} \tag{2.4}$$

in the case of the Δ_L decays. Here Γ denotes the decay rates of the corresponding processes. At the tree level, these asymmetries vanish, but they yield a non-zero contribution at the one-loop level. The leading order contribution comes from the interference between the tree-level diagrams shown in Figs. 2.1(a) and 2.2(a) and one-loop diagrams shown in Figs. 2.1(b)–(d) and 2.2(b). RHN decays then contribute by [20, 43]

$$\begin{aligned}\epsilon_{N_R^i} = &- \frac{1}{8\pi}\frac{1}{(Y_\nu Y_\nu^\dagger)_{ii}}\sum_j \mathrm{Im}\left[(Y_\nu Y_\nu^\dagger)_{ij}^2\right] f\left(\frac{M_j^2}{M_i^2}\right) - \\ &- \frac{1}{2\pi M_i}\frac{1}{(Y_\nu Y_\nu^\dagger)_{ii}}\mathrm{Im}\left[(Y_\nu)_{ij}(Y_\nu)_{ik}(Y_\Delta^*)_{jk}\mu\right] g_i,\end{aligned} \tag{2.5}$$

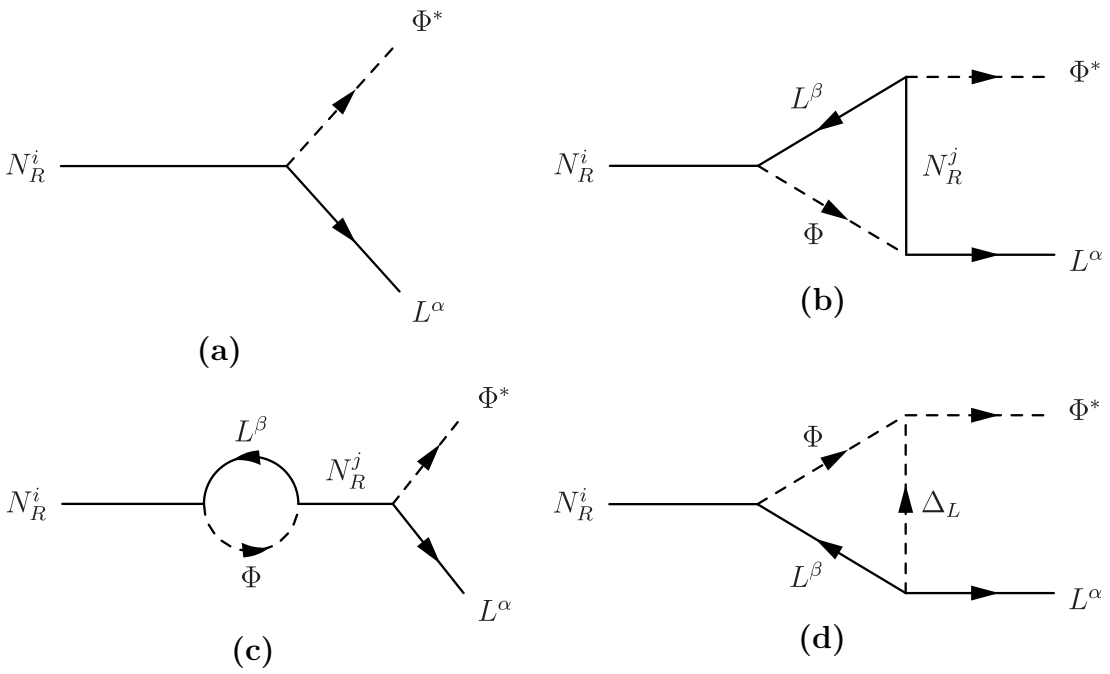

Figure 2.1: Feynman diagrams of RHN decays up to one-loop level that contribute to the CP asymmetry.

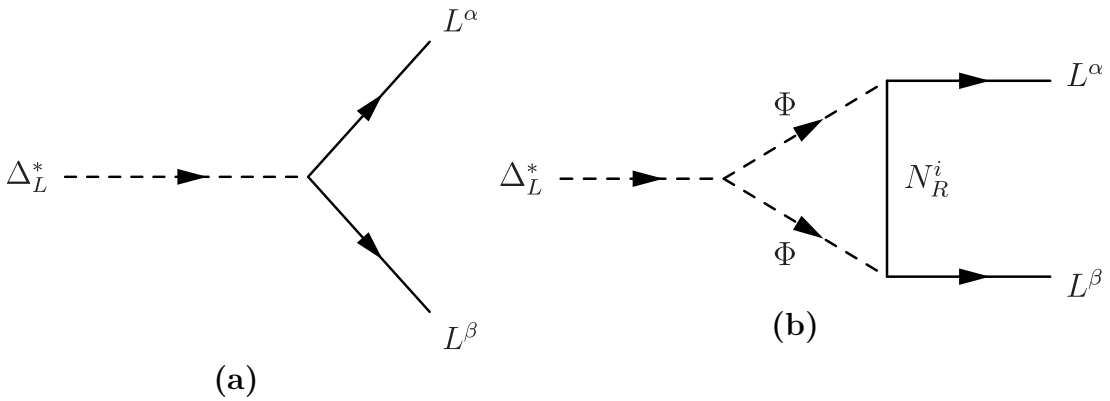

Figure 2.2: Feynman diagrams of Δ_L decays up to one-loop level that contribute to the CP asymmetry.

where M_i are RHN masses, the function $f(x)$ is defined as

$$f(x) = \sqrt{x}\left[-\frac{2-x}{1-x} + (1+x)\log\frac{1+x}{x}\right], \tag{2.6}$$

the factor g_i is defined as

$$g_i = \left[1 - \frac{M_\Delta^2}{M_i^2}\log\left(1 + \frac{M_i^2}{M_\Delta^2}\right)\right], \tag{2.7}$$

and the summation over the indices j and k is performed in the second term.

The first term in the formula (2.5) represents a well-known result, which can be commonly found in the literature, and it comes from the pure type-I seesaw extension. However, in the combination of seesaw types I and II, the CP asymmetry of the RHN decays also receives a contribution from the loop diagram shown in Fig. 2.1(d), which involves Δ_L in the loop. This contribution is represented by the second term in the formula (2.5).

The decay of Δ_L itself contributes by [20]

$$\epsilon_\Delta = \frac{1}{8\pi}\sum_i M_i \frac{\mathrm{Im}\left[(Y_\nu^*)_{ij}(Y_\nu^*)_{ik}(Y_\Delta)_{jk}\mu^*\right]}{\sum_{lm}\left|(Y_\nu)_{lm}\right|^2 M_\Delta^2 + |\mu|^2}\log\left[1 + \frac{M_\Delta^2}{M_i^2}\right], \tag{2.8}$$

again with the summation over the indices j and k.

Leptogenesis as formulated by Fukugita and Yanagida[2] [13] takes the advantages (in terms of Sakharov's conditions) arising from the seesaw extension – namely, that it entails LNV and CP violation – and provides an explanation for the baryon asymmetry. Leptogenesis is a mechanism that generates a net lepton number in the C and CP-violating OOE decays of RHNs and Δ_L in the hot early Universe. The net lepton number is subsequently partially converted into a baryon asymmetry by the non-perturbative sphaleron processes that violate $B + L$ and conserve $B - L$.

2.4 Evolution equations for leptogenesis

2.5 Boltzmann equations

In the hot primordial plasma, which is simultaneously subjected to cooling and dilution due to the Hubble expansion, there are continuous creation, annihilation, decay and scattering of particles, until some of these processes stop once the plasma reaches the energy threshold for a given process, or the expansion rate becomes comparable to the rate of the process. Therefore, it is necessary to carry out the statistics of processes over the whole primordial plasma.

As for leptogenesis, in addition to the above CP-violating decays of RHNs and Δ_L, other processes that RHNs and Δ_L may undergo need to be taken into account, since they may consequently affect the final asymmetry. One thus needs to solve appropriate Boltzmann equations (BEs) governing the evolution of the number densities and asymmetries of interest. To this end, we employ `ULYSSES` [44, 45], the numerical solver of BEs, which however to date solves

[2]They formulated the leptogenesis for RHNs only.

BEs for RHN-driven leptogenesis only and does not account for effects from Δ_L. This means that our approach is valid in the regime of dominant RHN-driven leptogenesis. We discuss the implications of this below. Technical details about the use of the `ULYSSES` are the subject of Section 4.1.3.

As an illustrative example, let us take the classical BEs for three decaying RHNs in the single flavour approximation [44]:

$$\begin{aligned}\frac{\mathrm{d}N_{N_R^i}}{\mathrm{d}z} &= -D_i\left(N_{N_R^i} - N_{N_R^i}^{\mathrm{eq}}\right),\\ \frac{\mathrm{d}N_{B-L}}{\mathrm{d}z} &= \sum_{i=1}^{3}\left[\epsilon_{N_R^i} D_i\left(N_{N_R^i} - N_{N_R^i}^{\mathrm{eq}}\right) - W_i N_{B-L}\right],\end{aligned} \tag{2.9}$$

where $z = M_1/T$ is a dimensionless evolution parameter with T being the temperature of the plasma, $N_{N_R^i}$ is the number density of the i-th heavy neutrino mass eigenstate N_R^i with $i = 1, 2, 3$, and $N_{N_R^i}^{\mathrm{eq}}$ then denotes the corresponding equilibrium value, with all number densities normalised to a comoving volume containing one photon [33, 44],

$$N_{N_R^i}^{\mathrm{eq}} \equiv N_{N_R^i}^{\mathrm{eq}}(z) = \frac{3}{8} x_i z^2 \mathcal{K}_2(z_i), \tag{2.10}$$

where

$$x_i = \frac{M_i^2}{M_1^2}, \quad z_i = \sqrt{x_i} z \tag{2.11}$$

and $\mathcal{K}_\alpha(z_i)$ are modified Bessel functions of the second kind, so that $N_{N_R^i}^{\mathrm{eq}}(z \ll 1) = 3/4$. N_{B-L} is the $B-L$ asymmetry. The final $B-L$ asymmetry is then $N_{B-L}^f \equiv N_{B-L}(z \gg 1)$. $\epsilon_{N_R^i}$ is defined by Eq. (2.5) ignoring the contribution from Δ_L. D_i is the decay term – the decay rate rescaled in the following way [33]

$$D_i \equiv D_i(z) = K_i x_i z \frac{\mathcal{K}_1(z_i)}{\mathcal{K}_2(z_i)}, \tag{2.12}$$

where K_i is the decay parameter defined as the ratio of the N_R^i decay width $\Gamma(N_R^i)$ to the Hubble expansion rate $H(T = M_i)$ [34, 46]. With the Hubble rate given by [33]

$$H(z) \approx 1.66\sqrt{g_*}\frac{M_1^2}{M_{Pl}}\frac{1}{z^2}, \tag{2.13}$$

where $g_* = 106.75$ is the number of relativistic degrees of freedom, and $M_{Pl} = 1.22 \times 10^{19}\,\mathrm{GeV}$ is the Planck mass; K_i can be expressed as follows [34, 46]

$$K_i \equiv \frac{\Gamma(N_R^i)}{H(T = M_i)} = \frac{v^2}{m_* M_i}(Y_\nu Y_\nu^\dagger)_{ii} = \frac{\tilde{m}_1}{m_*}, \tag{2.14}$$

where $m_* \approx 10^{-3}\,\mathrm{eV}$ [46] is the equilibrium neutrino mass and $\tilde{m}_1$ is the effective neutrino mass[3]. W_i is the washout term given by [33]

$$W_i \equiv W_i(z) = \frac{1}{4} K_i \sqrt{x_i} z_i^3 \mathcal{K}_1(z_i). \tag{2.15}$$

[3]In the literature, two regimes are usually distinguished: weak ($\tilde{m}_1 < m_*$) and strong ($\tilde{m}_1 > m_*$) washout regimes [46]. The larger the decay parameter the stronger the washout.

The right-hand side of BEs represents the reactions the RHNs undergo. In the hot plasma, at temperatures above the mass of the heaviest RHN, RHNs are created and their decays, represented by D_i in BEs, produce lepton asymmetry. Any lepton asymmetry is subsequently washed out by inverse decays (and other effects), represented by W_i (scattering, e.g., would contribute by another term, see Ref. [46]). As the Universe expands, the plasma cools down. Once the temperature drops below M_3, OOE decays of the heaviest RHNs start to produce a net asymmetry, because the thermal bath does not have enough energy for inverse decays. However, the asymmetry is still partially washed out by inverse decays of lighter RHNs. The scheme repeats until the mass threshold M_1 is reached.

In this sense, ignoring Δ_L means that we are in a specific regime, where Δ_L decays early enough, i.e. the mass M_Δ is large enough, that any asymmetry produced by it (cf. Eq. (2.8)) is washed out by RHNs and its loop contribution to the RHN decays (the second term in Eq. (2.5)) is negligible. Thus at least one RHN have to be much lighter than Δ_L. This means, in other words, that the decay rate of Δ_L have to be way bigger than the decay rate of N_R^i, i.e. $\Gamma(\Delta_L) \gg \Gamma(N_R^i)$, where [20, 47]

$$\Gamma(\Delta_L) = \frac{1}{8\pi} M_\Delta \left(\frac{|\mu|^2}{M_\Delta^2} + \sum_{ij} |(Y_\Delta)_{ij}|^2 \right), \tag{2.16}$$

and

$$\Gamma(N_R^i) = \frac{1}{8\pi} M_i (Y_\nu Y_\nu^\dagger)_{ii}. \tag{2.17}$$

This leads to the following constraints on the parameter space [47]

$$M_\Delta \left(\frac{|\mu|^2}{M_\Delta^2} + \sum_{ij} |(Y_\Delta)_{ij}|^2 \right) \gg M_i (Y_\nu Y_\nu^\dagger)_{ii}. \tag{2.18}$$

2.5.1 Flavour effects and density matrix equations

When considering the simplest case of N_R^1 dominated leptogenesis, the classical BEs provide a suitable description [46]. However, in SO(10)-inspired models, e.g., leptogenesis is dominated by N_R^2 [33, 48, 49]. Consideration of heavier RHNs requires different sets of BEs specific to different RHN mass patterns [50]. Moreover, BEs fail in the transition regimes for $M_i \sim 10^9$ GeV and $M_i \sim 10^{12}$ GeV [50].

Furthermore, the CP asymmetry can be significantly modified by flavour effects [50].Consider the decoherence effects. The lepton and antilepton states $|L^i\rangle$ and $|\overline{L^\alpha}\rangle$, respectively, originating from the N_R^i decays can be expressed as a linear combination of flavour eigenstates L^α ($\overline{L^\alpha}$) with $\alpha = e, \mu, \tau$,

$$|L^i\rangle = \sum_\alpha C_{i\alpha} |L^\alpha\rangle, \quad |\overline{L^i}\rangle = \sum_\alpha \overline{C}_{i\alpha} |\overline{L^\alpha}\rangle, \tag{2.19}$$

where the amplitudes $C_{i\alpha}$ and $\overline{C}_{i\alpha}$, although in general $C_{i\alpha} \neq \overline{C}_{i\alpha}$ [33, 50], are given at tree level by [33, 50]

$$C_{i\alpha} = \overline{C}_{i\alpha} = \frac{Y_{\alpha i}^*}{\sqrt{(YY^\dagger)_{ii}}}. \tag{2.20}$$

For $M_1 \gg 10^{12}\,\mathrm{GeV}$, the states $|L^i\rangle$ and $|\overline{L^\alpha}\rangle$ evolve coherently [33], i.e. there is a coherence between their production and inverse decays. For $M_1 < 10^{12}\,\mathrm{GeV}$, the coherent evolution breaks down due to the interactions with electroweak bosons [33, 34] and the states $|L^i\rangle$ and $|\overline{L^\alpha}\rangle$ transform into a pure flavor states.

To account for flavour effects, instead of classical BEs such as (2.9), more general density matrix equations (DME) need to be employed. BEs (2.9) then need to be replaced by [33, 44, 50]

$$\begin{aligned}
\frac{\mathrm{d}N_{N_R^i}}{\mathrm{d}z} &= -D_i\left(N_{N_R^i} - N^{\mathrm{eq}}_{N_R^i}\right), \\
\frac{\mathrm{d}(N_{B-L})_{\alpha\beta}}{\mathrm{d}z} &= \sum_{i=1}^{3}\left[(\epsilon_{N_R^i})_{\alpha\beta}D_i\left(N_{N_R^i} - N^{\mathrm{eq}}_{N_R^i}\right) - \frac{1}{2}W_i\{P^{0(i)}, N_{B-L}\}_{\alpha\beta}\right] \\
&\quad - \frac{\Gamma_\tau}{2Hz}\left[\begin{pmatrix}1&0&0\\0&0&0\\0&0&0\end{pmatrix}, \left[\begin{pmatrix}1&0&0\\0&0&0\\0&0&0\end{pmatrix}, N_{B-L}\right]\right]_{\alpha\beta} \\
&\quad - \frac{\Gamma_\mu}{2Hz}\left[\begin{pmatrix}0&0&0\\0&1&0\\0&0&0\end{pmatrix}, \left[\begin{pmatrix}0&0&0\\0&1&0\\0&0&0\end{pmatrix}, N_{B-L}\right]\right]_{\alpha\beta},
\end{aligned}$$

where the second line now represents the equation for the $B-L$ asymmetry matrix in the charged lepton flavour basis. The CP asymmetry of the decays of N_R^i is unlike the previous case described by the matrix $(\epsilon_{N_R^i})_{\alpha\beta}$ [33],

$$\begin{aligned}
(\epsilon_{N_R^i})_{\alpha\beta} = \frac{3i}{32\pi(Y_\nu Y_\nu^\dagger)_{ii}}\sum_{j\neq i}\Bigg[&\frac{\xi(x_j/x_i)}{\sqrt{x_j/x_i}}(Y^*_{i\alpha}Y_{j\beta}(Y_\nu Y_\nu^\dagger)_{ji} - Y_{i\beta}Y^*_{j\alpha}(Y_\nu Y_\nu^\dagger)_{ij}) + \\
&+ \frac{2}{3(x_j/x_i - 1)}(Y^*_{i\alpha}Y_{j\beta}(Y_\nu Y_\nu^\dagger)_{ij} - Y_{i\beta}Y^*_{j\alpha}(Y_\nu Y_\nu^\dagger)_{ji})\Bigg]
\end{aligned} \tag{2.21}$$

where $\xi(x)$ as defined in Ref. [33] can be expressed using Eq. (2.6) as follows

$$\xi(x) = \frac{2}{3}\sqrt{x}f(x). \tag{2.22}$$

$P^{0(i)}_{\alpha\beta}$ is the projection matrix [33],

$$P^{0(i)}_{\alpha\beta} = C_{i\alpha}C^*_{i\beta} = \frac{Y^*_{i\alpha}Y_{i\beta}}{(Y_\nu Y_\nu^\dagger)_{ii}}, \tag{2.23}$$

and terms proportional to [33]

$$\frac{\Gamma_\alpha}{2Hz} = \frac{8\times 10^{-3}y_\alpha^2 T}{Hz} \tag{2.24}$$

are related to the charged lepton interactions.

The baryon asymmetry is then given by [34, 44, 46]

$$\eta_B = \frac{a_{\mathrm{sph}}}{f}\,\mathrm{Tr}\,N^f_{B-L} \simeq 0.013\,\mathrm{Tr}\,N^f_{B-L}, \tag{2.25}$$

where $a_{\mathrm{sph}} = 28/79$ [44] is the SM sphaleron factor, the fraction of N^f_{B-L} converted into a baryon asymmetry by sphaleron processes, and $f = N_\gamma^{\mathrm{rec}}/N_\gamma^0 = 27$ [44, 46] is

the dilution factor caused by the photon production from the onset of leptogenesis until recombination. In the literature [46], one may encounter an expression using the efficiency factor κ_f which is independent of CP asymmetry. If we also assume that leptogenesis is dominated by decays of one of the RHNs, then

$$\eta_B \sim \frac{3}{4}\frac{a_{\text{sph}}}{f}\epsilon_{N_R^i}\kappa_f \simeq 0.96 \times 10^{-2}\epsilon_{N_R^i}\kappa_f \lesssim 0.013\frac{2\epsilon_{N_R^i}}{K_i}, \tag{2.26}$$

However, even DME (2.21) are not the most general possible evolution equations for leptognesis, there are many other effects that could potentially influence the final asymmetry. E.g., research by Hahn-Woernle et al. [51] has shown, among other things, that dropping assumption of kinetic equilibrium[4] has minimal impact on the evolution of number densities and lepton asymmetry, and that the inclusion of quantum statistics can enhance the final asymmetry by up to 50 % in the weak washout regime, while it can suppress the final asymmetry by up to 20 % in the strong washout regime (the stronger washout the milder effect). It is important to note that these results are based on single RHN decay approximation.

Despite what has been said, BEs provide a solid foundation for modeling leptogenesis, but one has to keep in mind possible uncertainties within few tens of percent.

[4]This assumption allows the BEs to be integrated over momentum space, and reaction rates to be thermally averaged, resulting in simpler equations that track only the number densities of particles rather than their full phase space distributions.

3. Flavour structure of Grand Unified Theories

3.1 Motivation for Grand Unified Theories

Attempts to provide a full-fledged description of phenomena that are (or could be) manifestations of physics beyond the SM (by which we particularly mean non-zero neutrino masses and the BAU) have led to mechanisms such as the seesaw mechanism (Chap. 1), baryogenesis, and leptogenesis (Chap. 2), that entail baryon and lepton number violating (BLNV) processes or the emergence of high-energy scales like M_i (In Sec. 4.3, we will mention that leptogenesis provide a lower bound for M_1, which is $10^9\,\mathrm{GeV}$).

Interestingly enough, a hint of high-energy dynamics is already visible at the pure SM level, namely, in the convergence of the running gauge couplings. These findings pave the way towards extensions, embedding the SM gauge group $\mathrm{SU}(3)_c \times \mathrm{SU}(2)_L \times \mathrm{U}(1)_Y$ into larger symmetry groups, and the concept of Grand Unified Theories (GUTs) [25].

From this perspective, GUTs, due to the fact that they incorporate BLNV [25], appear to be a natural framework for leptogenesis[1]. Note that, based on Eqs. (2.5) and (2.21), in order to solve BEs (2.9) and (2.21), the neutrino Yukawa coupling Y_ν is required. However, it is largely undetermined – when expressed in the physical Casas-Ibarra parametrization [23], one finds out that out of 18 parameters, only 5 have been determined from experiments so far (3 lepton mixing angles and the light neutrino mass squared differences). Consequently, the neutrino Yukawa matrix is largely undetermined. However, a defining feature of GUTs is that the corresponding symmetry group is larger compared to the SM one, and thus more predictive, which is manifested by correlations between different types of Yukawa couplings or their symmetricity. This has profound implications, especially if the Yukawa couplings are fitted to the known values of the low-energy data, thereby strictly constraining the parameter space for Y_ν and, consequently, leptogenesis.

Let us now briefly describe the concept of GUTs and the version we investigated in our research.

3.2 Brief introduction to Grand Unified Theories

As mentioned above, the GUTs are an attempt for unified description of particles and their interactions. Within the GUT framework, this means merging all the SM gauge couplings at a high-energy scale M_{GUT} into a single coupling associated with a simple non-Abelian group and, subsequently, breaking this symmetry group down to the SM.

To achieve gauge coupling unification, one must solve the renormalization group equations (RGEs) in order to link values of the running gauge couplings

[1]Note that leptogenesis is not a unique prediction of a single theory, but rather a generic consequence of various extensions of the SM that incorporate LNV processes.

at different energy scales – the values we know [52] at the electroweak scale $M_{\mathrm{Z}} = 91.1876\,\mathrm{GeV}$,

$$g_s(M_Z) = 1.2104 \pm 0.0051, \tag{3.1}$$
$$g(M_Z) = 0.65100 \pm 0.00028, \tag{3.2}$$
$$g'(M_Z) = 0.357254 \pm 0.000069, \tag{3.3}$$

and those at the GUT scale M_{GUT} determined from the unification condition. The couplings g_s, g and g' correspond, respectively, to the factors of the SM gauge group $\mathrm{SU}(3)_c \times \mathrm{SU}(2)_L \times \mathrm{U}(1)_Y$.

It is important to note that this procedure does not guarantee successful unification within any simple non-Abelian group into which the SM is embedded. For instance, let us consider the simplest SM extension in terms of the GUT, the Georgi-Glashow model based on the symmetry group SU(5) [24]. In this model, gauge couplings do not unify without the inclusion of further intermediate-scale dynamics such as supersymmetry (SUSY). Despite the appealing features of SUSY, it is not favored by experimental observations. Then it is natural to search for a larger non-SUSY group. These typically exhibit complicated spontaneous symmetry breaking (SSB) through multiple intermediate stages.[2]

3.3 Non-SUSY SO(10)

In this work, we focus on the models based on the non-SUSY SO(10), as these are the most promising candidates for a realistic GUT. The SO(10) gauge group not only possesses both the aforementioned properties – it contains the SM as a subgroup and provides a framework for gauge couplings unification – but also accommodates all fermions of a given generation, including RHNs, into a single multiplet, the 16-dimensional irreducible spinor representation $\mathbf{16}_F$.

Regarding the SSB, it is realized, as in the SM, by Higgs scalars. SO(10) can be spontaneously broken down to the SM through various breaking chains (cf. e.g., [26, 53]), necessitating the construction of an appropriate scalar sector to achieve the desired symmetry breaking pattern while remaining consistent with experimental observations.

3.4 Yukawa sector of non-SUSY SO(10)

The allowed content of the Yukawa sector of non-SUSY SO(10) stems from the following decomposition of the direct product $\mathbf{16}_F \times \mathbf{16}_F$,

$$\mathbf{16}_F \times \mathbf{16}_F = \mathbf{10} + \overline{\mathbf{126}} + \mathbf{120}. \tag{3.4}$$

Thus, the most general Yukawa Lagrangian is given by

$$\mathcal{L}_{Yukawa}^{general} = \mathbf{16}_F(Y_{10}\mathbf{10}_H + Y_{126}\overline{\mathbf{126}}_H + Y_{120}\mathbf{120}_H)\mathbf{16}_F, \tag{3.5}$$

[2] Above the lowest intermediate breaking scale, it no longer makes sense to talk about the couplings g_s, g and g' as the physics there is effectively governed by a different symmetry group with its own couplings.

where $\mathbf{10}_H$, $\overline{\mathbf{126}}_H$, and $\mathbf{120}_H$ are 10-, 126-, and 120-dimensional scalar representations.

For the purposes of this work, we require the model to be realistic and minimal in terms of the number of free parameters (as each scalar enters the model with at least one Yukawa coupling structure). We would also like to somehow implement the seesaw mechanism for generating non-zero neutrino masses (1.8). Such a minimal and potentially realistic Yukawa sector typically contains the scalar representations $\mathbf{10}_H$ and $\overline{\mathbf{126}}_H$ (cf. Ref. [30], which provides a comprehensive analysis of the scalar sector of non-SUSY renormalisable SO(10)). In the following lines we only briefly motivate the proposed construction of the Yukawa sector:

1. Since one cannot write down the Majorana mass term as in Eq. (1.1) above the scale of the $B - L$ symmetry breaking, $\overline{\mathbf{126}}_H$ is essential, as it breaks $\mathrm{SU}(2)_R$, thereby enabling the implementation of the seesaw mechanism.

2. For the fermionic mixing, at least one additional multiplet is needed. We have chosen $\mathbf{10}_H$, although an alternative in the form of $\mathbf{120}_H$ is also viable, cf. [30].

3. To obtain a realistic fermionic spectrum, both the $\overline{\mathbf{126}}_H$ and the $\mathbf{10}_H$ representations have to be complex. This means that $\mathbf{10}_H$, which is originally real, needs to be complexified.

The Yukawa Lagrangian of such a minimal potentially realistic model is thus given by:

$$\mathcal{L}_{Yukawa} = \mathbf{16}_F(Y_{10}\mathbf{10}_H + Y_{126}\overline{\mathbf{126}}_H + \tilde{Y}_{10}\mathbf{10}^*_H)\mathbf{16}_F, \tag{3.6}$$

with the Yukawa couplings Y_{10}, Y_{126} and $\tilde{Y}_{10}$ being 3×3 complex symmetric matrices in the flavour space. One can choose a basis where, e.g., Y_{10} is real and diagonal, thereby ending up with 27 parameters in total.

The Yukawa couplings from the above Lagrangian (3.6) can be matched to those of the EFT valid below M_{GUT}. In this work, we effectively consider a direct breaking of SO(10) to the SM

$$\mathrm{SO}(10) \xrightarrow{M_{\mathrm{GUT}}} \mathrm{SU}(3)_c \times \mathrm{SU}(2)_L \times \mathrm{U}(1)_Y \xrightarrow{M_{\mathrm{Z}}} \mathrm{SU}(3)_c \times \mathrm{U}(1)_Q, \tag{3.7}$$

without any intermediate stages[3]. Consequently, the Yukawa couplings of the GUT model (3.6) are to be matched directly to those of the SM (cf. the construction in [33, 53, 54]):

$$vY_u = v_u^{10}Y_{10} + v_d^{10*}\tilde{Y}_{10} + v_u^{126}Y_{126}, \tag{3.8}$$
$$vY_d = v_d^{10}Y_{10} + v_u^{10*}\tilde{Y}_{10} + v_d^{126}Y_{126}, \tag{3.9}$$
$$vY_\nu = v_u^{10}Y_{10} + v_d^{10*}\tilde{Y}_{10} - 3v_u^{126}Y_{126}, \tag{3.10}$$
$$vY_e = v_d^{10}Y_{10} + v_u^{10*}\tilde{Y}_{10} - 3v_d^{126}Y_{126}, \tag{3.11}$$
$$M_R = v_R^{126}Y_{126}, \tag{3.12}$$
$$M_L = v_L^{126}Y_{126}, \tag{3.13}$$

[3]One can look at it also in such a way that possible intermediate symmetry-breaking scales are effectively placed at M_{GUT} (cf. [26]).

where Y_u, Y_d, and Y_e are the Yukawa matrices for the up- and down-type quarks, and the charged leptons, respectively. Y_ν and M_R are the neutrino Yukawa matrix and the Majorana mass matrix for RHNs, respectively, from the type-I seesaw (1.2), and M_L is the mass matrix of the left-handed scalar triplet from the type-II seesaw (1.6). At the same time, adhering to the so-called extended survival hypothesis [26, 55], we assume that only those scalars are present that acquire a VEV in the current or later stage of the SSB. In the above Eqs. (3.8)–(3.13) these VEVs are represented by complex weights v_u^{10}, v_d^{10}, v_u^{126}, v_d^{126}, v_R^{126} and v_L^{126},

$$\begin{aligned} v_u^{10,126} &= \langle (1,2,-1/2)_{10,126} \rangle, \qquad & v_d^{10,126} &= \langle (1,2,+1/2)_{10,126} \rangle \\ v_R^{126} &= \langle (1,1,0)_{126} \rangle, & v_L^{126} &= \langle (1,3,+1)_{126} \rangle \end{aligned} \tag{3.14}$$

where the superscripts refer to associated scalar representation and the numbers in parentheses stem from the decomposition of the representations $\mathbf{10}_H$ and $\overline{\mathbf{126}}_H$ [33] with respect to the SM gauge group $\mathrm{SU}(3)_c \times \mathrm{SU}(2)_L \times \mathrm{U}(1)_Y$.

The SM Higgs field is encompassed in a mixture of $\mathbf{10}_H$ and $\overline{\mathbf{126}}_H$, VEVs then have to fulfill the following normalization

$$\sqrt{|v_u^{10}|^2 + |v_d^{10}|^2 + |v_u^{126}|^2 + |v_d^{126}|^2 + 2\,|v_L^{126}|^2} = \sqrt{2}v = 246\,\mathrm{GeV}. \tag{3.15}$$

In the literature, one can commonly encounter the subsequent step of imposing a global Peccei-Quinn symmetry $U(1)_{PQ}$ [29, 30, 32]:

$$\mathbf{16}_F \to e^{i\alpha}\mathbf{16}_F, \quad \mathbf{10}_H \to e^{-2i\alpha}\mathbf{10}_H, \quad \overline{\mathbf{126}}_H \to e^{-2i\alpha}\overline{\mathbf{126}}_H, \tag{3.16}$$

where α is a real parameter. Reasons for doing this are that it solves the strong CP problem, it may provide the axionic dark matter [31] and it further simplifies the Yukawa Lagrangian (3.6) to:

$$\mathcal{L}_{Yukawa}^{+PQ} = \mathbf{16}_F(Y_{10}\mathbf{10}_H + Y_{126}\overline{\mathbf{126}}_H)\mathbf{16}_F \tag{3.17}$$

thereby enhancing the predictive power and resulting in the following relations:

$$vY_u = v_u^{10}Y_{10} + v_u^{126}Y_{126}, \tag{3.18}$$
$$vY_d = v_d^{10}Y_{10} + v_d^{126}Y_{126}, \tag{3.19}$$
$$vY_\nu = v_u^{10}Y_{10} - 3v_u^{126}Y_{126}, \tag{3.20}$$
$$vY_e = v_d^{10}Y_{10} - 3v_d^{126}Y_{126}, \tag{3.21}$$
$$M_R = v_R^{126}Y_{126}, \tag{3.22}$$
$$M_L = v_L^{126}Y_{126}. \tag{3.23}$$

It is important to note that correlations (3.8)–(3.13) and (3.18)–(3.23) are valid only at the GUT scale. Below the GUT scale, Y_u, Y_d, Y_e, Y_ν, M_R, and M_L evolve according to RGEs of the SM extended by RHNs and Δ_L, see Appendix B.

4. Methodology and numerical analysis

Now with all the theoretical ingredients at hand, we can proceed to the main task of this work: to verify whether non-SUSY SO(10), specifically models (3.6) and (3.17) described in previous chapter, are able to reproduce the experimentally measured low-energy data while simultaneously generate a sufficiently large baryon asymmetry (2.2). Given the high complexity of the problem, we resort to solving it numerically.

4.1 Fitting procedure

4.1.1 Minimization of χ^2

We need to compare a model prediction $X_i^{\text{pred.}}(\mu)$ for an i-th observable with the observation $\overline{X}_i(\mu)$, where μ is the energy scale. To quantify the discrepancy between $X_i^{\text{pred.}}(\mu)$ and $\overline{X}_i(\mu)$ we compute the χ^2 function

$$\chi^2 = \sum_i^N \left(\frac{X_i^{\text{pred.}}(\mu) - \overline{X}_i(\mu)}{\sigma_i(\mu)} \right)^2 = \sum_i^N p_i^2, \tag{4.1}$$

where σ_i are the errors of experimental measurements and p_i are the corresponding pulls. By minimizing χ^2, the model parameters are fitted to the observations.

For the minimization of χ^2, we employ a differential evolution (DE) algorithm [56, 57], which is capable to find the global minimum and it is well-suited for optimization of complex problems. This optimization method consists of sampling a set of points in the parameter space and iteratively improving it by the following procedure:

1. The function we want to minimize is $\chi^2 : \mathbb{R}^d \to \mathbb{R}$. Initialization consists in randomly generating a population of candidate solutions $\mathbf{x} \in \mathbb{R}^d$ in the searched parameter space (or part of it). The population size is kd, where k denotes the number of points per dimension. In the case of models (3.6) and (3.17), the dimension is $d = 35$ and $d = 23$, respectively. It is recommended to choose $k = 20$ or $k = 30$ for tricky functions, but smaller k is also possible for minimization of χ^2 [57]. It is important to keep in mind that the larger the population size, the more time-consuming it is to evaluate the function.

2. For each $\mathbf{x}$ in the population, the algorithm does the following steps:

   (a) Three other distinctive candidates $\mathbf{a}$, $\mathbf{b}$ and $\mathbf{c}$ are chosen randomly from the population.

   (b) A random index I is chosen from the set $\{1, ..., d\}$.

   (c) For each component of a given $\mathbf{x}$, a number $r_i = \text{rand}(0, 1)$ is chosen.

(d) If $r_i < C_r$ or $i = I$, the i-th component of a new candidate solution $\mathbf{y}_i$ is computed as follows:

$$\mathbf{y}_i = \mathbf{a}_i + F(\mathbf{b}_i - \mathbf{c}_i), \tag{4.2}$$

otherwise $\mathbf{y}_i = \mathbf{x}_i$. Here $C_r \in (0, 1)$ is the cross-over rate and F is the differential weight. In our case, $F = \mathrm{rand}(0.5, 1.0)$.

(e) If $\chi^2(\mathbf{y}) \leq \chi^2(\mathbf{x})$, $\mathbf{x}$ is replaced by $\mathbf{y}$.

Step 2. is repeated until a satisfactory result is achieved.

4.1.2 Low-energy data

We compare the predictions $X_i^{\mathrm{pred.}}(\mu)$ of the SO(10) models against the low-energy data of the SM observables and the baryon-to-photon number density ratio (2.1), which are listed in Tab. 4.1. Actually, when comparing $X_{\eta_B}^{\mathrm{pred.}}$ and $\overline{X}_{\eta_B}$, we do not need to adhere strictly to the precision within 1σ error. At the end of Sec. 2.4, we briefly discussed that including other effects may modify η_B within a few tens of percent. So, we allow for these possible uncertainties. In particular, we would like to get at least close to the correct order of magnitude of η_B, since the estimate from the SM is ten orders of magnitude smaller. However, in this way, predictions of much smaller orders of magnitude (such as 10^{-20}) are not adequately penalized in χ^2 compared to predictions that are, let say, by only one or two orders of magnitude smaller than the experimental value (2.2). Therefore we fit the decimal logarithm of the value (2.2) (cf. Tab. 4.1) in order the algorithm to be sensitive to order of magnitude of η_B. At the same time we estimate the corresponding 1σ error to be roughly $\log 2$.

Regarding the remaining quantities in Tab. 4.1, the quark and charged-lepton masses, along with the Higgs quartic coupling, are taken from [52], and the CKM parameters from [58]. Concerning the neutrino mass ordering, we consider only the normal ordering. The corresponding mass squared differences, along with lepton mixing angles, are adopted from NuFIT 5.2 [59] results from November 2022, available on http://www.nu-fit.org. The adopted values are based on measurements withnout Super-Kamiokande atmospheric neutrino data. For reader's interest, the same for inverted neutrino mass ordering can be found therein, and for an examination of the effect of mass ordering within the framework of SO(10), we refer to [28].

Particular attention should be paid to uncertainties of these quantities. First, comprehensive analysis (cf. [59, 60]) shows that the one-dimensional χ^2 projection for $\sin^2\theta_{23}^{\mathrm{PMNS}}$ has two local minima around the global χ^2 minimum. Although only the best fit from NuFIT is listed in Tab. 4.1, we reflect this fact in our analysis by involving the proper one-dimensional χ^2 projection for $\sin^2\theta_{23}^{\mathrm{PMNS}}$ (depicted in Figure 4.1, the corresponding dataset is available on http://www.nu-fit.org). Then we interpret the pull of $\sin^2\theta_{23}^{\mathrm{PMNS}}$ as the square root of the relevant contribution to χ^2 and we determine the sign with respect to the best fit:

$$p_{\sin^2\theta_{23}^{\mathrm{PMNS}}} = \mathrm{sgn}\left[X^{\mathrm{pred.}}_{\sin^2\theta_{23}^{\mathrm{PMNS}}}(\mu) - \overline{X}_{\sin^2\theta_{23}^{\mathrm{PMNS}}}(\mu)\right] \cdot \sqrt{\Delta\chi^2} \tag{4.3}$$

Second, the uncertainties of some quantities in Tab. 4.1 (denoted by an asterisk) are enlarged so that they are not less than 1 % of the corresponding central values.

Observable	$\overline{X}_i$	σ_i
m_u [MeV]	1.23	0.21
m_c [GeV]	0.620	0.017
m_t [GeV]	168.3	1.7*
m_d [MeV]	2.67	0.19
m_s [MeV]	53.16	4.61
m_b [GeV]	2.839	0.028*
$\sin\theta_{12}^{\mathrm{CKM}}$	0.2251	0.0023*
$\sin\theta_{13}^{\mathrm{CKM}}/10^{-3}$	3.71	0.14
$\sin\theta_{23}^{\mathrm{CKM}}/10^{-2}$	4.180	0.067
δ_{CKM}	1.143	0.011*
Δm_{21}^2 [$10^{-5}\mathrm{eV}^2$]	7.41	0.21
Δm_{31}^2 [$10^{-3}\mathrm{eV}^2$]	2.511	0.028
m_e [MeV]	0.4831	0.0048*
m_μ [GeV]	0.1018	0.0010*
m_τ [GeV]	1.729	0.017*
$\sin^2\theta_{12}^{\mathrm{PMNS}}$	0.303	0.012
$\sin^2\theta_{13}^{\mathrm{PMNS}}/10^{-2}$	2.203	0.059
$\sin^2\theta_{23}^{\mathrm{PMNS}}$	0.572	0.023†
λ	0.5579	0.0056*
$\log\eta_B$	−9.21	0.30

* Errors that have been enlarged so that they are not less than 1 % of the corresponding central values.

† The best fit from NuFIT, but $\sin^2\theta_{23}^{\mathrm{PMNS}}$ has two local minima.

Table 4.1: Overview of measured SM observables with their central values and corresponding 1σ errors at the electroweak scale M_Z along with η_B.

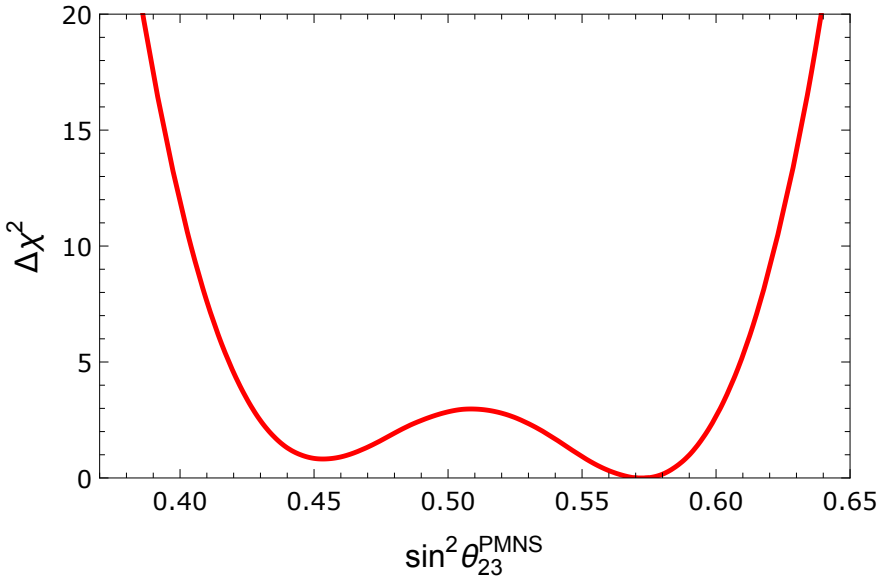

Figure 4.1: One-dimensional χ^2 projection for $\sin^2\theta_{23}^{\mathrm{PMNS}}$ with two local minima.

The reason for this is that according to Eq. (4.1), the greater the precision with which a quantity is measured, the larger its weight in the χ^2. This means that, e.g. charged-lepton masses would have a dominant influence as they are measured with significantly greater precision than the other quantities. By enlarging the errors, we ensure a more balanced contribution of all observables to the χ^2. Moreover, it can be assumed that the χ^2 minimum for the original σ's can be found in the vicinity of the points obtained in this way.

4.1.3 Model prediction

Role of renormalization group running

We have not yet looked at how to make the model prediction $X_i^{\mathrm{pred.}}(\mu)$. As already mentioned in Section 3.2 and tacitly reflected in Eq. (4.1), one has to deal with running parameters. The physics above the GUT scale is expressed in terms of Y_{10}, Y_{126} and possibly $\tilde{Y}_{10}$. The SM extended with RHNs and Δ_L governs the physics after SSB, i.e. below the GUT scale, and it is expressed in terms of Y_u, Y_d, Y_e, Y_ν, M_R, and M_L. These Yukawa matrices of different models can be translated into each other using the matching relations (3.8)–(3.13) or (3.18)–(3.23), which are valid at the GUT scale. These relations are thus crucial both for transitioning between the high- and low-energy parameters and for constraining the parameter space of the SO(10).

Once a specific set of Y_{10}, Y_{126} (and $\tilde{Y}_{10}$) of SO(10) is selected, one can translate them into Yukawa matrices of extended SM and then extract the SM observables as usual. However, their values are thus obtained at the GUT scale, let us say at $M_{\mathrm{GUT}} \sim 10^{16}\,\mathrm{GeV}$, whereas they are to be compared with values in Tab. 4.1, which are at the M_Z scale, i.e. at scale fourteen orders of magnitude lower. This requires solving a set of coupled RGEs for the EFT valid below the GUT scale, i.e. in our case the SM with RHNs and Δ_L. These RGEs are listed in Appendix B. For solving RGEs and for extracting the SM observables

from Yukawa matrices, we use the available `REAP/MixingParameterTools` package [61] for `Mathematica`. At the same time, we work in a scheme in which the running of VEVs can be ignored.

The form of RGEs reflects the sequence of sub-GUT EFTs, and is influenced also by the field content. One can choose from various setups – regarding the particular symmetry-breaking chain, the position of intermediate breaking scales that may be other free parameters, position of M_{GUT}, and a type of the seesaw mechanism.

Further, we consider both contributions to neutrino masses, i.e. the combination of seesaw types I and II (1.8). Consequently, regarding the field content, in addition to the fields already present in the pure SM, we have to take into account the heavy RHNs and the heavy Δ_L. Here comes a limitation of `REAP`. Although `REAP` includes a package of RGEs for SM with 3 heavy RHNs, it does not include the effects of Δ_L – neither the running of Y_Δ nor the type-II seesaw mechanism are included. Nevertheless, the effect of Δ_L on the running seems to be small across different fits [29, 62], and seesaw type II can be imitated using a non-zero κ at M_{GUT}, see Eqs. (A.5) and (A.6).

Once the RGEs are defined, we can proceed to the fitting procedure of model parameters. There are two opposing approaches to fitting the model to low-energy data: bottom-up and top-down approach. In the bottom-up approach, we start from low-energy data, evolve them through RGEs up to high energies and there we minimize χ^2. The advantage is that we start from well-known values. On the other hand, there is an ambiguity in reconstruction of Yukawa matrices from these values (e.g., we have to ensure the Yukawa matrices Y_{10} and Y_{126} to be symmetric). And there are other disadvantages. We do not know how the uncertainties evolve to high energies. This would require employment of Monte-Carlo sampling of points into 1σ intervals of low-energy data and to evolve these points, thereby mapping the 1σ errors to the high-energy scale. Further, we do not know at which scales to add the heavy fields. And finally, this approach is useless for symmetry breaking with intermediate breaking stages.

In the top-down approach, we start from a high-energy theory, evolve the parameters down to low energies and there we minimize χ^2. Thus, we do not know what values to start from. Then one has to sample points randomly at high energies, for each of them compute RGEs and repeat this procedure iteratively until a satisfactory fit is achieved. On the other hand, this approach properly takes into account the thresholds at which heavy fields are integrated out and it is applicable to general symmetry breaking chains. In our analysis, we perform the top-down approach.

Prediction for the baryon asymmetry

In Sec. 2.4, we introduced the formalism for leptogenesis in terms of BEs (2.9) or DME (2.21) for evolution of number densities $N_{N_R^i}$ and $B-L$ asymmetry N_{B-L}. These equations have to be solved in order to obtain the yield of leptogenesis. The relation between η_B and N^f_{B-L} is given by Eq. (2.25).

As already mentioned above, for numerical solution of BEs, we employ python package `ULYSSES` [44, 45]. In our analysis, we use the model in `ULYSSES` labeled as `3DME` [44, 50] together with the default settings for initial conditions, which

means that we set the initial abundances of RHNs and lepton asymmetry number densities to zero. The `3DME` model provides DME (2.21).

Inputs for `ULYSSES` are the Yukawa matrix Y_ν at $B-L$ breaking scale $M_{B-L} \sim M_3$ and RHN masses M_i. It is important to note here that Y_ν evolves like other parameters according to RGEs, but this running is not incorporated in `ULYSSES`. Nevertheless, the evolution is solved over $z \in \langle 10^{-1}, 10^2 \rangle$, i.e. $T \in \langle 10 M_1, 10^{-2} M_1 \rangle$. At leading order, we can neglect such a short running of three orders.

4.2 Strategy of the fitting procedure

Let us summarize schematically our strategy of the fitting the model parameters to low-energy data:

1. We sample points in the parameter space of the SO(10) models (3.6) and (3.17) at $M_{\rm GUT} = 2 \times 10^{16}$ GeV. This part is described in detail in the next Sec. 4.3.

2. Using the matching conditions (3.8)–(3.13) or (3.18)–(3.23) and Eqs. (A.5) and (A.6), we construct the SM Yukawa matrices and Y_ν, M_R, and κ at $M_{\rm GUT}$.

3. For all sampled points, we solve RGEs from $M_{\rm GUT}$ to $M_{\rm Z}$, numerically using the `REAP` package. In particular, we solve two-loop RGEs of Y_u, Y_d, Y_e, and λ, and one-loop RGEs of Y_ν, M_R, and κ (since the two-loop version is not yet available). The list of RGEs is in Appendix B.

4. We send Yukawa matrices Y_ν at the seesaw scale $M_{B-L} \sim M_3$ and RHN masses M_i as inputs to `ULYSSES` and compute η_B.

   It is important to consider at this step whether BEs needs to be solved for every point and during the whole fitting procedure, as the evolution of BEs is more time demanding than the RGE evolution. One may choose from two options:

   (a) η_B is included in the computation of χ^2. This means that the points are pushing to a region of the parameter space with both good flavour fits and good η_B. In this case, we have no choice but to compute η_B in every iteration. Nevertheless, for wrong flavour fits, we do not need to have precise η_B. Instead, it would be more efficient to estimate η_B e.g. from Eq. (2.26) without turning on `ULYSSES` and start to compute full-fledged BEs or DME after achieving good enough χ^2.

   (b) η_B is not included in the computation of χ^2. This means that the points are pushing to a region of the parameter space with good flavour fits independent of η_B. In this case, it is most efficient to compute η_B after the fitting procedure. This approach reveals η_B in the region of the best flavour fit.

5. At the $M_{\rm Z}$ scale, we construct the SM observables using the `MixingParameterTools` package. Apart from that listed in Tab. 4.1, we can construct

observables which have not yet been measured (such as $\delta_{\rm CP}$ or light neutrino masses) and thus make a prediction for future experiments.

6. The predictions for quark and charged-lepton masses, quark and leptonic mixing angles, CKM phase, neutrino mass squared differences, Higgs quartic coupling, and possibly $\log_{10}\eta_B$ are then compared with values in Tab. 4.1 by computing the χ^2 function.

7. To find the parameter values that provide the best fit to the measured data, we employ the optimization algorithm of differential evolution. It finds a new better generation of points. The procedure is then repeated from point 1. until a satisfactory fit is achieved. We use $\chi^2/n \leq 1$ as the condition for satisfactory fit, where n is the number of observables.

8. We scan the region of the parameter space around the minimum of χ^2. To this end, we iterate the above procedure further and track all sampled points, thus collecting a set of satisfactory configurations. We add another step: once a point achieves a certain threshold, it is stored and substituted by a random configuration with perturbed inputs.

4.3 Parameter space

4.3.1 Gauge couplings

An integral part of the procedure described above is to define the parameter space and how to explore it efficiently.

Regarding the SM gauge couplings, we perform a bottom-up approach to evolve their values (3.1), (3.2) and (3.3) at $M_{\rm Z} = 91.1876\,\text{GeV}$ up to $M_{\rm GUT} = 2\times10^{16}\,\text{GeV}$ using two-loop RGEs (B.2), (B.3), and (B.11) together with an approximation that the leading Yukawa-sector contribution to the gauge β-functions at the two-loop level comes from the top Yukawa coupling (cf. Eq. (B.11)), i.e.,

$$Y_u \sim \frac{1}{v}\begin{pmatrix}0&0&0\\0&0&0\\0&0&m_t\end{pmatrix}, \quad Y_d \sim Y_e \sim Y_\nu \sim \begin{pmatrix}0&0&0\\0&0&0\\0&0&0\end{pmatrix}. \tag{4.4}$$

The seesaw parameters can be estimated in this very crude approximation as follows:

$$\kappa \sim \begin{pmatrix}0&0&0\\0&0&0\\0&0&0\end{pmatrix}, \quad M_R \sim M_{\rm GUT}\begin{pmatrix}1&0&0\\0&1&0\\0&0&1\end{pmatrix} \tag{4.5}$$

And we use the low-energy value of λ, see below.

In this way, we obtain very accurate values of the gauge couplings at $M_{\rm GUT}$, the variations of which and impact of these variations on other parameters caused by the evolution of full-fledged RGEs back to $M_{\rm Z}$ would be next-to-leading-order effect. Thus we can fix the following high-energy values of gauge couplings (in the convention (B.1)) obtained by just described bottom-up approach

$$g_3(M_{\rm GUT}) = 0.5237, \quad g_2(M_{\rm GUT}) = 0.5226, \quad g_1(M_{\rm GUT}) = 0.5803, \tag{4.6}$$

and use them as fixed initial conditions for the subsequent top-down evolution of full-fledged RGEs. Otherwise they should properly be part of the fitting procedure.

Moreover, as a by-product one gets a naive guess on the top Yukawa coupling and λ at M_{GUT}

$$y_t(M_{\mathrm{GUT}}) \approx 0.417, \quad \lambda(M_{\mathrm{GUT}}) \approx -0.044. \tag{4.7}$$

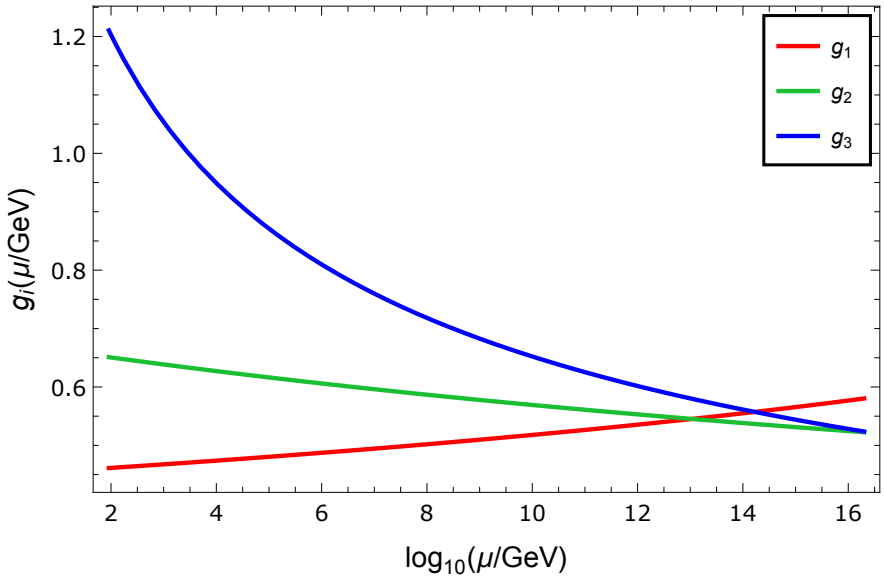

Figure 4.2: Two-loop running of the SM gauge couplings.

4.3.2 Fitted parameters

The main inputs are the Yukawa matrices Y_{10}, Y_{126} and possibly $\tilde{Y}_{10}$ at M_{GUT}, VEVs, and λ. For the Yukawa matrices, we decompose each of their elements into an absolute value and a phase. We sample the latter uniformly from $\langle 0, 2\pi \rangle$, but instead of absolute values, we sample uniformly their logarithmic values. At the same time, we work in the basis where Y_{10} is a real and positive diagonal matrix and Y_{126} and $\tilde{Y}_{10}$ are complex symmetric matrices.

Generally complex VEVs v_u^{10}, v_d^{10}, v_u^{126}, and v_d^{126} can be chosen such that v_u^{10} and v_d^{10} are real and v_u^{126} and v_d^{126} are complex. We decompose the complex ones into an absolute value and a phase. The remaining VEVs v_R^{126} and v_L^{126} are real.

Except for v_R^{126}, these VEVs have to be sampled so as to satisfy the normalization (3.15). So, we fix one of these VEVs, namely v_u^{10} (we have this freedom thanks to the normalization condition), generate the remaining ones and normalize them according to the Eq. (3.15). At the same time the normalization (3.15) implies that absolute values of these VEVs lie in the interval $\langle 0, 246 \rangle$ GeV. However, based on previous research [29], v_L^{126} seems to be very small, so its upper bound can be set much lower. On the other hand, v_R^{126} is assumed to be extremely large, since it corresponds to the seesaw scale. Thus, we sample v_R^{126} and v_L^{126} from the logarithmic distribution: $\log(v_R^{126}/\mathrm{GeV}) \in \langle 11, 15 \rangle$ and $\log(v_L^{126}/\mathrm{GeV}) \in \langle -16, -6 \rangle$.

The absolute values and phases of the remaining VEVs are sampled uniformly from $\langle 0, 246\rangle$ GeV and $\langle 0, 2\pi\rangle$, respectively.

Further, we assume, that Y_{10} is hierarchical,

$$(Y_{10})_{11} \lesssim (Y_{10})_{22} \lesssim (Y_{10})_{33}, \tag{4.8}$$

which in combination with the assumption that the SM Higgs projection is predominantly in v_u^{10} and concerning our guess for top-quark Yukawa coupling (4.7) give

$$(Y_{10})_{33} \sim y_t(M_{\rm GUT}). \tag{4.9}$$

Thus Y_{10} can be sampled as follows:

$$-8 \lesssim \log(Y_{10})_{11} \lesssim \log(Y_{10})_{22} \lesssim \log(Y_{10})_{33}, \quad -1 \lesssim \log(Y_{10})_{33} \lesssim 0. \tag{4.10}$$

In the case of Y_{126}, we do not have such straightforward constraints. First, the perturbativity has to be maintained. Second, based on Eq. (3.12), Y_{126} says something about the mass spectrum of RHNs. One can do the Takagi decomposition of the Yukawa matrix Y_{126}, $Y_{126}^{\rm diag.} = U^T Y_{126} U$; then $v_R^{126} Y_{126}^{\rm diag.}$ corresponds to the mass spectrum of the RHNs. We assume hierarchical RHNs[1],

$$M_1 < M_2 < M_3 \lesssim v_R^{126} \leftrightarrow (Y_{126}^{\rm diag.})_{11} < (Y_{126}^{\rm diag.})_{22} < (Y_{126}^{\rm diag.})_{33} \lesssim 1. \tag{4.11}$$

Moreover, in this case, leptogenesis suggests a lower bound on the mass of the lightest of the RHNs – the Davidson-Ibarra limit [43]:

$$M_1 \gtrsim 10^9\,{\rm GeV}. \tag{4.12}$$

When sampling Y_{126}, we shall take into account constraints (4.11) and (4.12).

In the case of $\tilde{Y}_{10}$, we have just the perturbativity condition. We have no constraints on phases of elements of Y_{126} and $\tilde{Y}_{10}$.

Last but not least, we can make the following estimate. In the model (3.17), one gets from Eqs. (3.19) and (3.21) the following relation

$$\mathrm{Tr}\left(Y_d Y_d^\dagger\right) + \frac{1}{3}\mathrm{Tr}\left(Y_e Y_e^\dagger\right) = \frac{4}{3}\mathrm{Tr}\left(Y_{10} Y_{10}^\dagger\right)\left|\frac{v_d^{10}}{v}\right|^2 + 4\mathrm{Tr}\left(Y_{126} Y_{126}^\dagger\right)\left|\frac{v_d^{126}}{v}\right|^2. \tag{4.13}$$

Evaluating the traces, one gets using Eq. (3.22)

$$\sum_{i=\{d,s,b\}} y_i^2 + \frac{1}{3}\sum_{i=\{e,\mu,\tau\}} y_i^2 = \frac{4}{3}\mathrm{Tr}\left(Y_{10} Y_{10}^\dagger\right)\left|\frac{v_d^{10}}{v}\right|^2 + \frac{4}{(v_R^{126})^2}\sum_{i=1}^{3} M_i^2 \left|\frac{v_d^{126}}{v}\right|^2, \tag{4.14}$$

which in the leading order gives

$$r_1^2 m_b^2(M_{\rm Z}) + \frac{r_2^2}{3} m_\tau^2(M_{\rm Z}) \simeq \frac{4}{3} y_t^2(M_{\rm GUT})\left|v_d^{10}\right|^2 + 4\left|v_d^{126}\right|^2, \tag{4.15}$$

where we expressed the relation in terms of known values – masses of bottom and τ at $M_{\rm Z}$, and y_t at $M_{\rm GUT}$ from the estimate (4.7). We introduced rescaling factors $r_1 \approx 0.4$ and $r_2 \approx 0.9$ coming from the running of bottom and τ Yukawa

[1] In resonant leptogenesis, RHNs are quasi-degenerate.

couplings, respectively, from M_{Z} to M_{GUT}. Since all terms in Eq. (4.15) are quadratic, one thus gets

$$\left|v_d^{10}\right| \lesssim 3.0\,\mathrm{GeV}, \tag{4.16}$$

$$\left|v_d^{126}\right| \lesssim 0.7\,\mathrm{GeV}. \tag{4.17}$$

These results should not be taken as constraints for $|v_d^{10}|$ and $|v_d^{126}|$, since we made some approximations. Nevertheless, they indicate that down-type VEVs may prefer small values. For potentially more efficient exploration, we can sample these VEVs in intervals (4.16) and (4.17).

The last remaining parameter is λ. We sample this parameter uniformly across the interval $\langle -0.5, 0.5 \rangle$.

5. Results

Before proceeding to the main results of our research, we would like to make a consistency check and test the ability of our code to reproduce earlier results. Our setup shares several features with that examined by Ohlsson and Pernow [29]. These include approximate breaking chain (3.7), the value of M_{GUT}, neutrino mass generation via the combination of seesaw types I and II, normal neutrino mass ordering, and the top-down approach employed for fitting. On the other hand, as far as only the flavour fits are concerned, the main differences are that we use low-energy data that has been updated since the article [29] was written and we impose more stringent threshold than Ohlsson and Pernow on their relative errors (1 % instead of 5 %). Further, for most of the parameters, we employ two-loop instead of one-loop RGEs and at the same time, we do not include the proper running of Δ_L. However, in the results of [29], Δ_L is integrated out right at the beginning of the RGE evolution, which is consistent with our approach.

In case of pure type-I seesaw mechanism and for the resulting high-energy parameters provided in the article, our code, despite the aforementioned differences, yields predictions that differ from those reported therein within 4 %, except for CKM phase δ_{CKM}, which seems to deviate by π. The situation is worse in case of the combined seesaw, where we are unable to reproduce reasonable χ^2.

5.1 Two-Yukawa model

5.1.1 Flavour fits

One of the main results of our research is the scan of the 23-dimensional parameter space of the model (3.17), a set of configurations consistent with the low-energy data listed in Tab. 4.1. This is also one of the main contributions of this thesis, as scientific papers usually report only the best fit (see, e.g., [28, 29, 62]).

In this sense, our research closely aligns with the research of Mummidi and Patel [33]. So, we will compare our results particularly with Ref. [33] throughout the subsequent discussion.

Yet there are some differences in both approaches. The authors of Ref. [33] consider the model (3.17) with the seesaw mechanism type I only and with the two-Higgs-doublet model (2HDM) as the sub-GUT EFT. At the same time, they employ the bottom-up approach using one-loop RGEs. The leptogenesis dynamics is described there by both numerical and analytical solutions of DME (2.21), the latter of which was derived under the assumption of N_R^2 dominated leptogenesis.

Figs. 5.1 and 5.2 show the set of approximately $63,000$ viable configurations projected onto the $\log(M_1/\mathrm{GeV})$-$\log(M_2/\mathrm{GeV})$ plane and the $\log(M_2/\mathrm{GeV})$-$\log(M_3/\mathrm{GeV})$ plane, respectively. From these flavour fits, η_B was excluded and those points were accepted that satisfy $\chi^2/n \leq 1$, where $n = 19$ and χ^2 is color-coded in the graphs. Although the dataset includes over $63,000$ points, it is not enough to fully cover the entire area where $\chi^2 \leq 19$, so the scan says nothing about bounds on the allowed ranges of parameters and predictions. Nevertheless, it indicates, e.g., the flavour fits to prefer hierarchical spectra of RHN masses, consistent with previous fits [29, 33]. However, our results suggest a preference

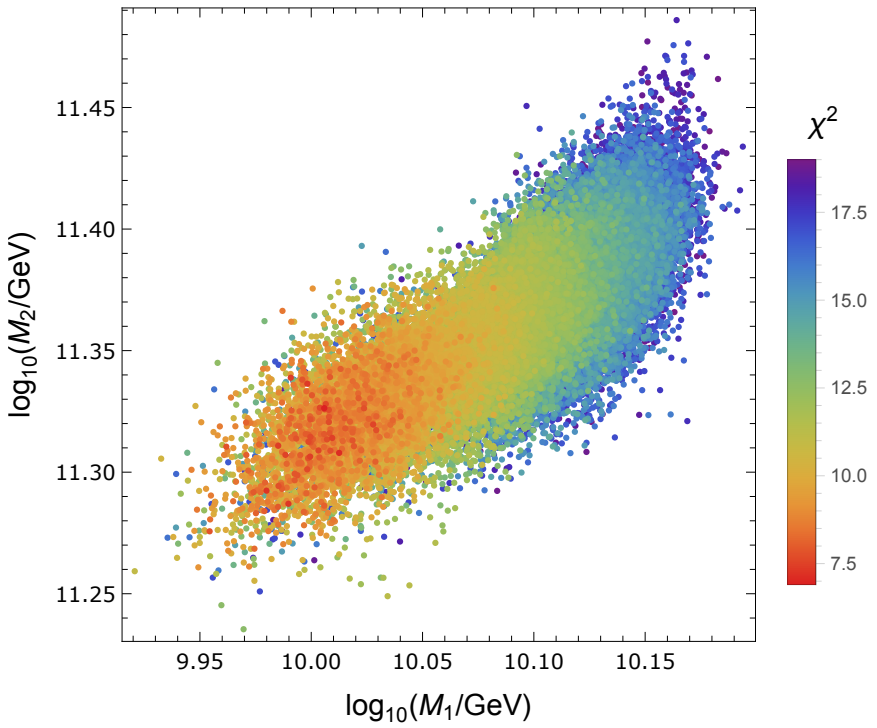

Figure 5.1: Configurations with $\chi^2 \leq 19$ in the 23-dimensional parameter space of the model (3.17) projected onto the $\log(M_1/\text{GeV})$-$\log(M_2/\text{GeV})$ plane where χ^2 is color-coded. For these flavour fits, η_B is not included in χ^2. The dataset shown contains approximately 63,000 configurations.

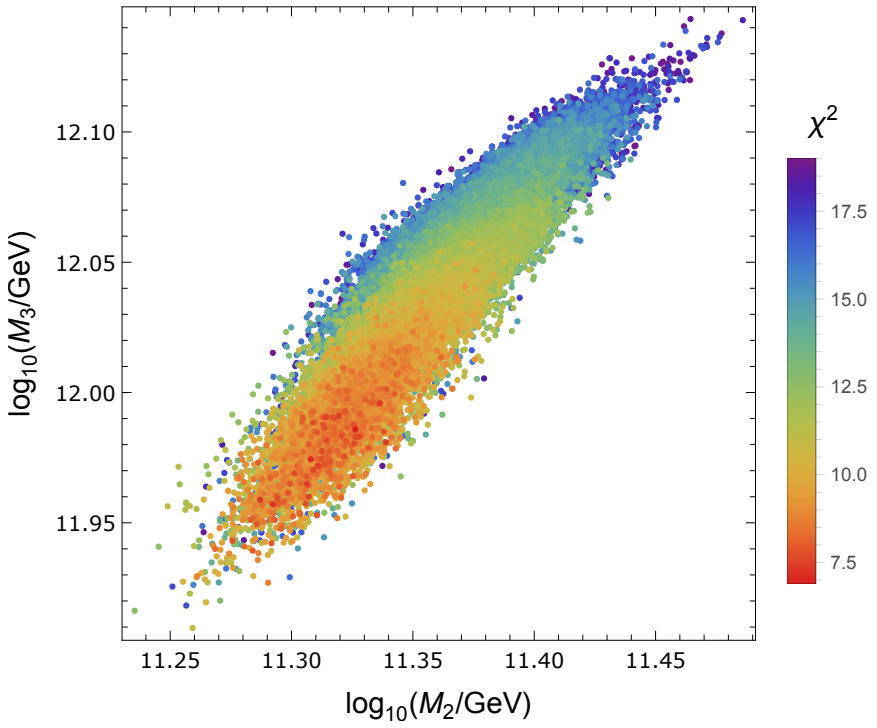

Figure 5.2: The same set of configurations as in Fig. 5.1 projected onto the $\log(M_2/\text{GeV})$-$\log(M_3/\text{GeV})$ plane where χ^2 is color-coded.

for heavier N_R^1 compared to [33].

In Tab. 5.1, we present the obtained ranges for the inputs in the used parame-

Parameter	Mean	σ
$\log_{10}(Y_{10})_{11}$	-3.7113	0.0098
$\log_{10}(Y_{10})_{22}$	-2.4555	0.0051
$\log_{10}(Y_{10})_{33}$	-0.5003	0.0032
$\log_{10}\lvert(Y_{126})_{11}\rvert$	-3.028	0.016
$\arg(Y_{126})_{11}$	5.848	0.024
$\log_{10}\lvert(Y_{126})_{12}\rvert$	-2.5148	0.0099
$\arg(Y_{126})_{12}$	4.679	0.020
$\log_{10}\lvert(Y_{126})_{13}\rvert$	-1.473	0.011
$\arg(Y_{126})_{13}$	2.7931	0.0078
$\log_{10}\lvert(Y_{126})_{22}\rvert$	-1.4403	0.0093
$\arg(Y_{126})_{22}$	0.0022	0.0016
$\log_{10}\lvert(Y_{126})_{23}\rvert$	-1.0391	0.0096
$\arg(Y_{126})_{23}$	3.8649	0.0085
$\log_{10}\lvert(Y_{126})_{33}\rvert$	-0.774	0.010
$\arg(Y_{126})_{33}$	0.286	0.034
v_u^{10}	244.397	0.062
v_d^{10}	3.635	0.024
$\lvert v_u^{126}\rvert$	27.79	0.55
$\arg v_u^{126}$	2.9491	0.0073
$\lvert v_d^{126}\rvert$	0.876	0.018
$\arg v_d^{126}$	2.8605	0.0090
$\log_{10} v_R^{126}$	12.728	0.032
$\log_{10} v_L^{126}$	-11.153	0.030
λ	-0.042	0.019

Table 5.1: Ranges for the inputs in the two-Yukawa model (3.17) obtained from the scan and reproducing satisfactory flavour fits. The inputs correspond to the used parametrization and VEVs are normalized according to Eq. (3.15).

trization (with VEVs normalized according to Eq. (3.15)) reproducing satisfactory

flavour fits with the best flavour fit being reproduced for

$$
\begin{aligned}
Y_{10} &= \begin{pmatrix} 1.998\times10^{-4} & 0 & 0 \\ 0 & 3.487\times10^{-3} & 0 \\ 0 & 0 & 0.3183 \end{pmatrix}, \\
Y_{126} &= \begin{pmatrix} (8.65-i4.45)\times10^{-3} & 6.3\times10^{-4}-i2.940\times10^{-2} & -0.3174+i0.1205 \\ 6.3\times10^{-4}-i2.940\times10^{-2} & 0.3509+i2.5\times10^{-4} & -0.675-i0.615 \\ -0.3174+i0.1205 & -0.675-i0.615 & 1.592+i0.410 \end{pmatrix}\times10^{-1}, \\
v_u^{10} &= 244.255\,\mathrm{GeV}, & v_d^{10} &= 3.609\,\mathrm{GeV}, \\
v_u^{126} &= (-28.59+4.95i)\,\mathrm{GeV}, & v_d^{126} &= (-0.862+0.2261i)\,\mathrm{GeV}, \\
v_R^{126} &= 4.69\times10^{12}\,\mathrm{GeV}, & v_L^{126} &= 2.98\times10^{-9}\,\mathrm{GeV},
\end{aligned}
\tag{5.1}
$$

where numbers of decimal digits stem from standard deviations of parameters in the dataset of obtained configurations.

Note, that there are 24 parameters in Tab. 5.1, but only 23 parameters were fitted. This is correct, because we used also normalization condition (3.15) reducing the number of free parameters by 1.

The predictions corresponding to the best fit are summarized in Tab. 5.2. It includes predictions and pulls for the SM observables and η_B. It also includes predictions for light and heavy neutrino masses and remaining parameters of PMNS matrix.

Based on Fig. 5.3, the dominant contributions to χ^2 come from the lepton

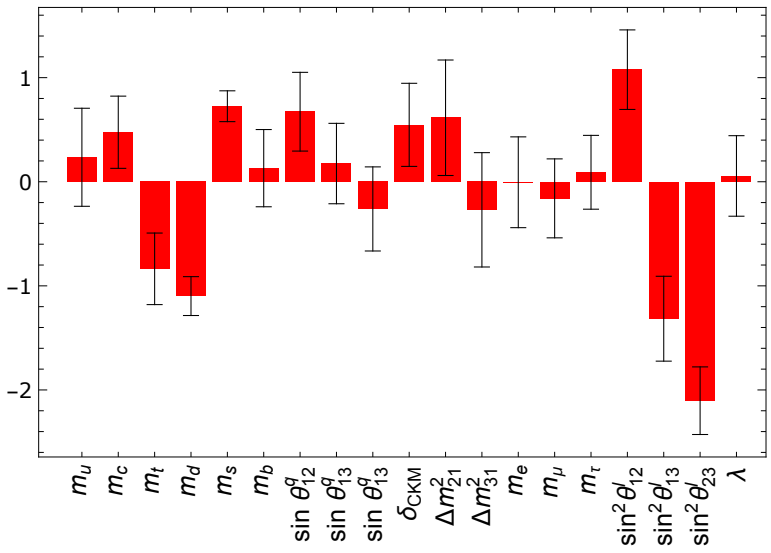

Figure 5.3: Pulls of the SM observables in the set of configurations from Figs. 5.1 and 5.2.

mixing angles and the down quark mass. In particular, it is worth mentioning the case of $\sin^2\theta_{23}^{\mathrm{PMNS}}$. Fig. 5.4, when comparing with Fig. 4.1, shows a strong preference for the second local minimum. This preference is indicated also by the best fit reported in Ref. [29], although the approach employed therein does

Observable	Prediction	Pull
m_u [MeV]	1.23	-7.24×10^{-3}
m_c [GeV]	0.632	0.686
m_t [GeV]	167.3	−0.593
m_d [MeV]	2.46	−1.08
m_s [MeV]	54.92	0.381
m_b [GeV]	2.841	0.0851
$\sin\theta_{12}^{\mathrm{CKM}}$	0.2250	−0.0363
$\sin\theta_{13}^{\mathrm{CKM}}/10^{-3}$	3.69	−0.148
$\sin\theta_{23}^{\mathrm{CKM}}/10^{-2}$	4.161	−0.276
δ_{CKM}	1.147	0.379
$\Delta m_{21}^2\,[10^{-5}\mathrm{eV}^2]$	7.54	0.613
$\Delta m_{31}^2\,[10^{-3}\mathrm{eV}^2]$	2.502	−0.315
m_e [MeV]	0.4843	0.253
m_μ [GeV]	0.1021	0.285
m_τ [GeV]	1.727	−0.117
$\sin^2\theta_{12}^{\mathrm{PMNS}}$	0.311	0.696
$\sin^2\theta_{13}^{\mathrm{PMNS}}/10^{-2}$	2.138	−1.10
$\sin^2\theta_{23}^{\mathrm{PMNS}}$	0.432	−1.48
λ	0.5573	−0.102
χ^2	−	6.93
$\log\eta_B$	−10.47	−4.19
m_1 [meV]	4.21	−
m_2 [meV]	9.65	−
m_3 [meV]	50.2	−
M_1 [GeV]	1.01×10^{10}	−
M_2 [GeV]	2.12×10^{11}	−
M_3 [GeV]	9.68×10^{11}	−
δ_{CP}	4.64	−
ϕ_1	5.16	−
ϕ_2	1.77	−

Table 5.2: Predictions obtained for the best fit of the two-Yukawa model (3.17) with $\chi^2 = 6.93$. In addition to the SM observables, several other predictions are also listed.

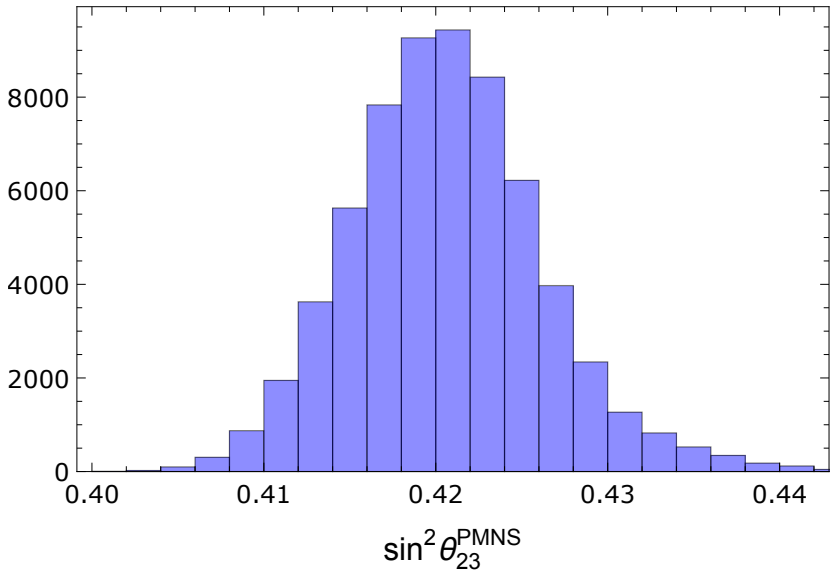

Figure 5.4: Histogram of $\sin^2\theta_{23}^{\mathrm{PMNS}}$ in the set of configurations from Figs. 5.1 and 5.2.

not account for the second local minimum. In contrast, Mummidi and Patel [33] report the best fit preferring the global minimum. This may be due to the fact that they not only do not take into account the shape of the one-dimensional χ^2 projection for $\sin^2\theta_{23}^{\mathrm{PMNS}}$ (Fig. 4.1), properly reflecting experimental measurements, but that they also use a different approach to RGE evolution than ours and [29].

Let us also provide here the histogram of $\log_{10}(v_R^{126}/\mathrm{GeV})$, see Fig. 5.5. When

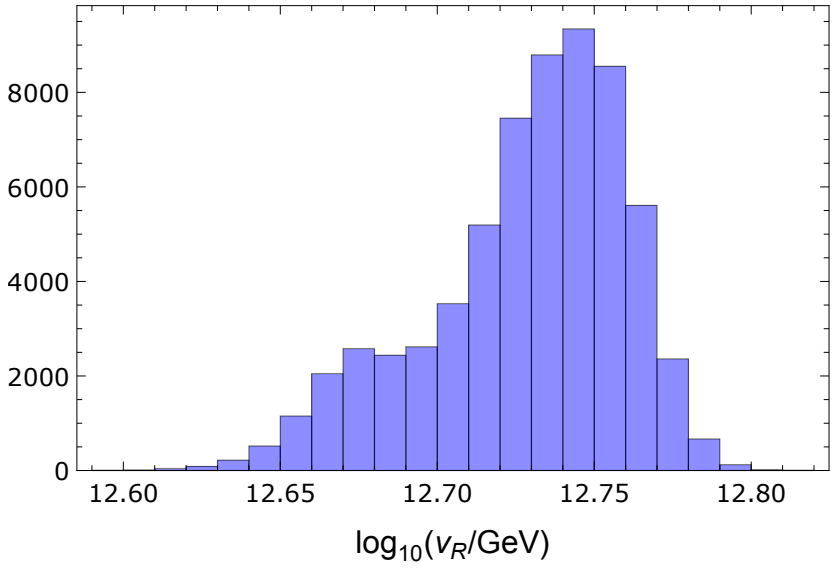

Figure 5.5: Histogram of $\log_{10}(v_R^{126}/\mathrm{GeV})$ in the set of configurations from Figs. 5.1 and 5.2. It is consistent with earlier results,

comparing it with histogram of $\log_{10}(v_L^{126}/\mathrm{GeV})$ in Fig. 5.6, one may notice, that both histograms complement each other as expected, in order to reproduce given light neutrino masses or, more precisely, mass-squared differences.

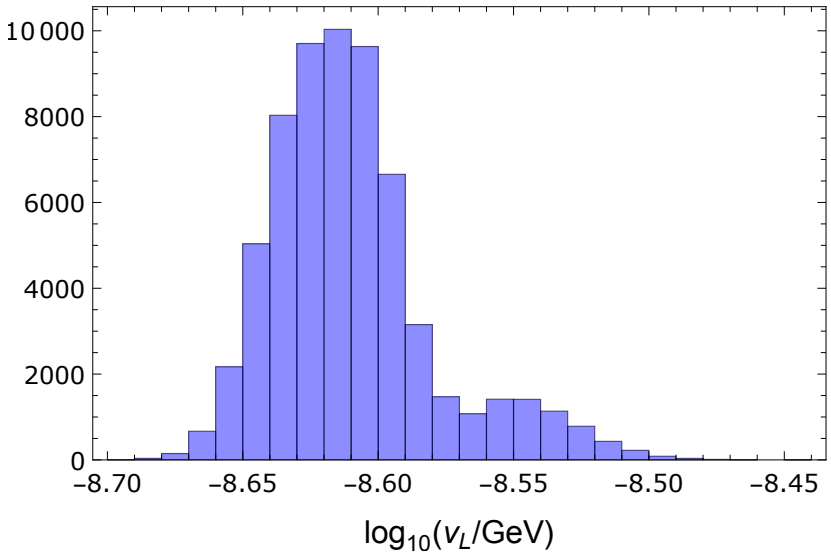

Figure 5.6: Histogram of $\log_{10}(v_L^{126}/\text{GeV})$ in the set of configurations from Figs. 5.1 and 5.2.

On the contrary, it is surprising that without explicitly solving full RGEs (considering full-fledged symmetry breaking pattern) taking into account correct running and unification of gauge couplings, i.e. without incorporation of $B-L$ breaking, we obtain the $B-L$ breaking scale consistent with earlier results that take into account proper running (cf. [26]).

Furthermore, based on the ranges of inputs in Tab. 5.1 (see also the inputs (5.1)), not only is matrix Y_{10} hierarchical, but matrix Y_{126} also shows some hierarchical structure. Regarding the VEVs, their values align with our guess on their hierarchy made in the previous chapter (cf. (4.16) and (4.17)).

5.1.2 Leptogenesis

When investigating successful leptogenesis, we focused on the case of pure flavour fits and glossed over why we did not pay attention to fits incorporating the yield of leptogenesis. Both of these approaches bring valuable information. The former case says something about the success of leptogenesis in the region of around the best flavour fit.

Figures 5.7 and 5.8 provide a complementary view to Figures 5.1 and 5.2, color-coding η_B of the viable configurations. Now, it is clear, why we did not pay attention to the fitting incorporating leptogenesis. Independently on the result of leptogenesis, pure flavour fits pushed the sampled points to the region with satisfactory η_B. Given the complexity of the studied problem, this seems like a miracle. It is important to remind that we only care about an order of magnitude agreement as used approximations may change the result by tens of percent.

When comparing Figs. 5.7 and 5.8 with the previously presented Figs. 5.1 and 5.2, one may notice that there are missing points, particularly in the bottom left corner in Figs. 5.7 and 5.8. Figs. 5.7 and 5.8 contain approximately $55,000$ configurations from the original dataset. The missing points are problematic, because η_B for these configurations is not reproducible on different computers

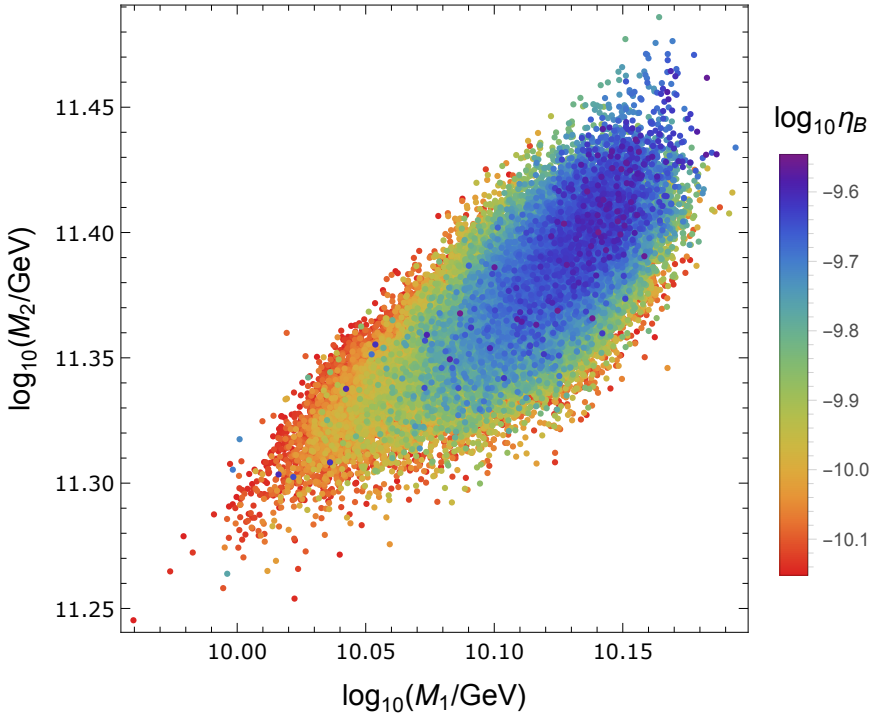

Figure 5.7: The same as in Fig. 5.1 with color-coded η_B. From the previous dataset, configurations in the unstable region are excluded. The dataset shown contains approximately 55, 000 configurations.

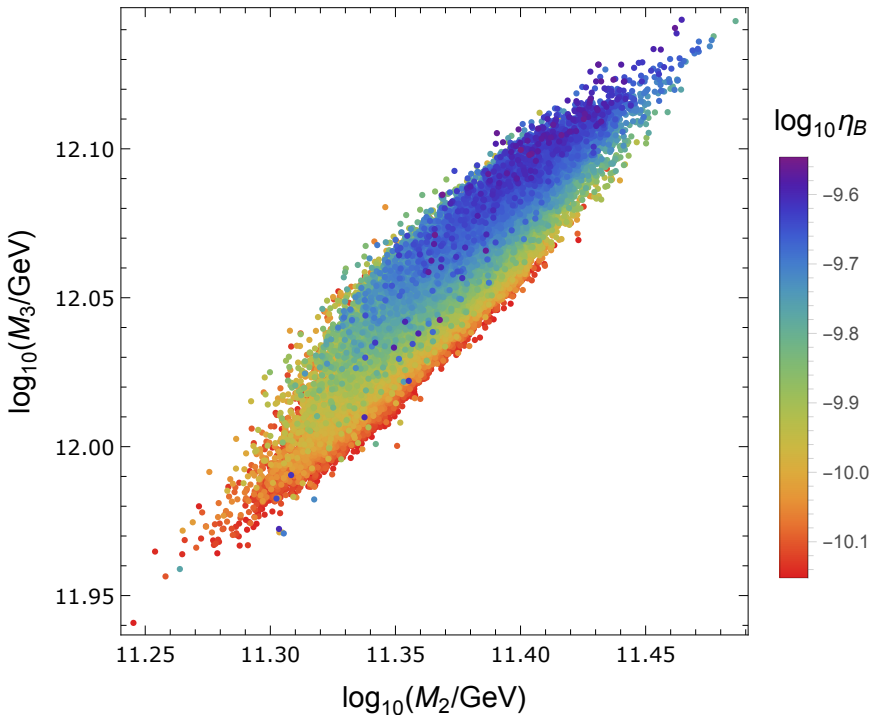

Figure 5.8: The same as in Fig. 5.7 with projection onto the $\log(M_2/\text{GeV})$-$\log(M_3/\text{GeV})$ plane.

(unlike RGE evolution). The results may differ by several orders of magnitude. This is a fundamental flaw of the employed procedure and it shows that there is a procedure in the code that depends on machine precision. If ULYSSES is unstable in this region of the parameter space, this would lead to the observed differences. Despite this complication, we have an extensive dataset.

As expected, Figs. 5.7 and 5.8 reveal trends opposite to that one in Figs. 5.1 and 5.2, since higher η_B requires heavier RHNs.

Fig. 5.9 then shows the evolution of $B-L$ asymmetries and η_B for the largest

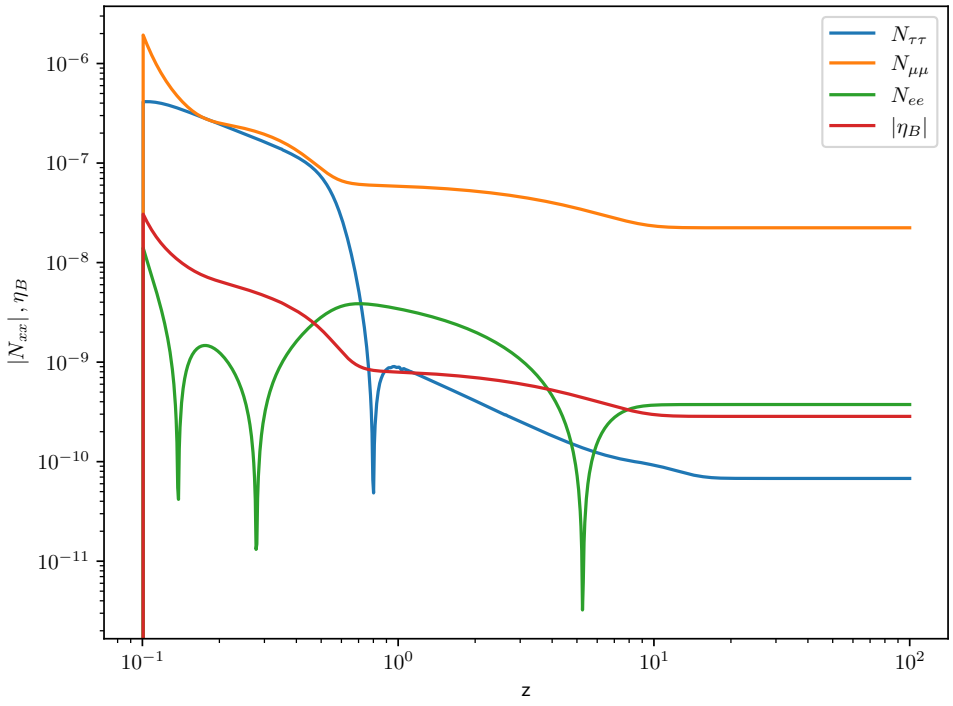

Figure 5.9: Solution of DME (2.21) for the largest η_B achieved in the set of configurations shown in Figs. 5.7 and 5.8.

final η_B achieved in the set of configurations shown in Figs. 5.7 and 5.8. It shows the dominant contribution from decays of the second lightest RHN as assumed by Mummidi and Patel [33]. The dominance of N_R^2 decays is also shown by Figs. 5.10, 5.11, 5.12, and 5.13. Figs. 5.10 and 5.12 show the CP asymmetries from N_R^1 and N_R^2 decays, respectively, computed from Eq. (2.5) for the original set of configurations shown in Figs. 5.1 and 5.2. For the same dataset, Figs. 5.11 and 5.13 show the washout for N_R^1 and N_R^2 decays, respectively. The decay parameter is computed from Eq. (2.14). Figs. 5.10 and 5.11 imply, based on Eq. (2.26), that N_R^1 decays themselves are unable to reproduce sufficiently high η_B and that their contribution to the total η_B is sub-dominant compared to N_R^2 decays (cf. Figs. 5.12 and 5.13).

5.2 Three-Yukawa model

It is already clear from previous results for two-Yukawa fits that the three-Yukawa model (3.6) has a solution – the previous one which can be reproduced for $\tilde{Y}_{10}$

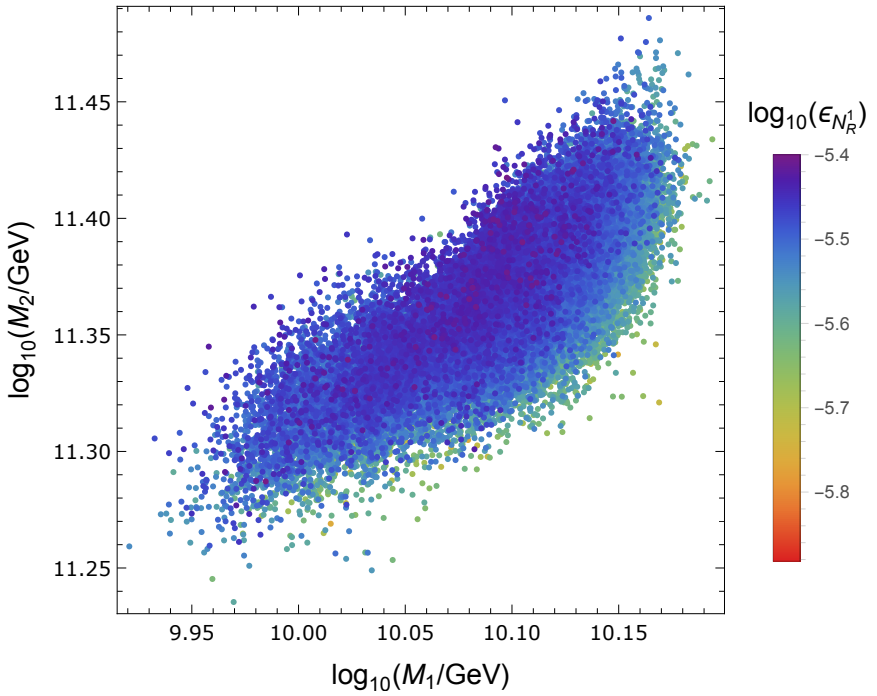

Figure 5.10: The CP asymmetry from N_R^1 decays for the set of configurations shown in Figs. 5.1 and 5.2.

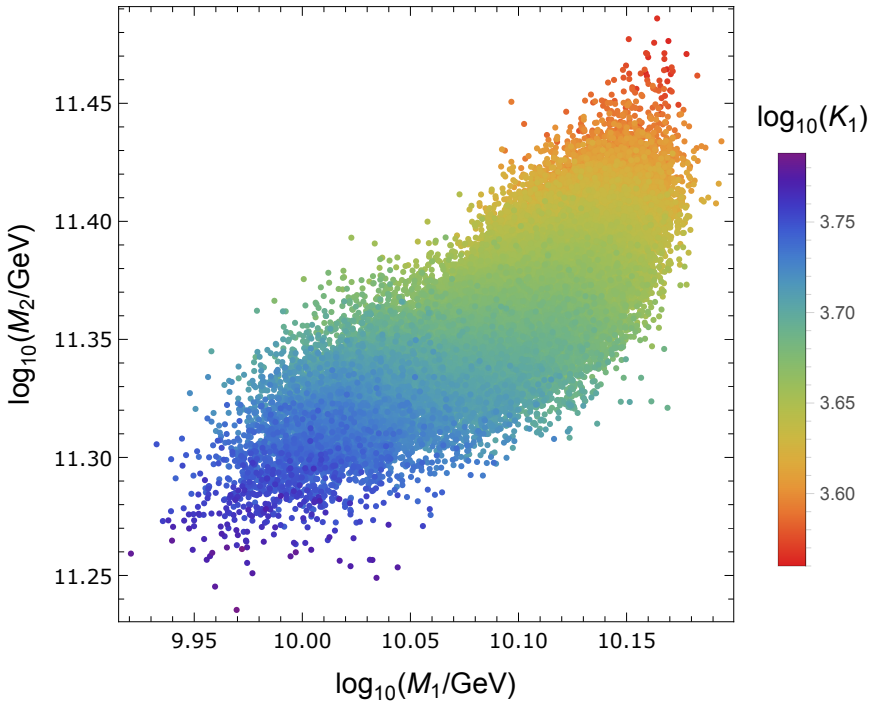

Figure 5.11: Washout in N_R^1 decays.

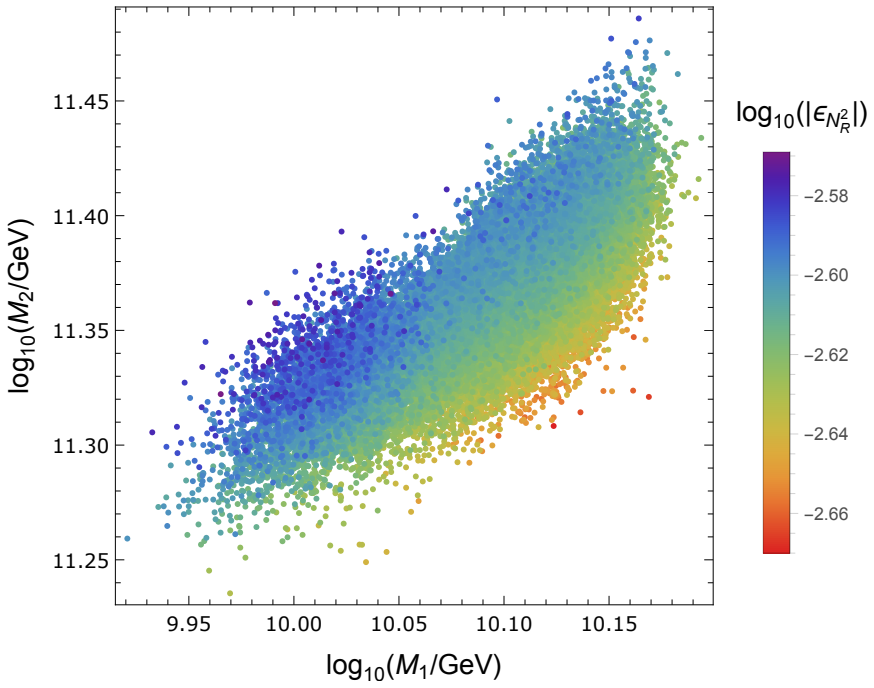

Figure 5.12: The CP asymmetry from N_R^2 decays for the set of configurations shown in Figs. 5.1 and 5.2.

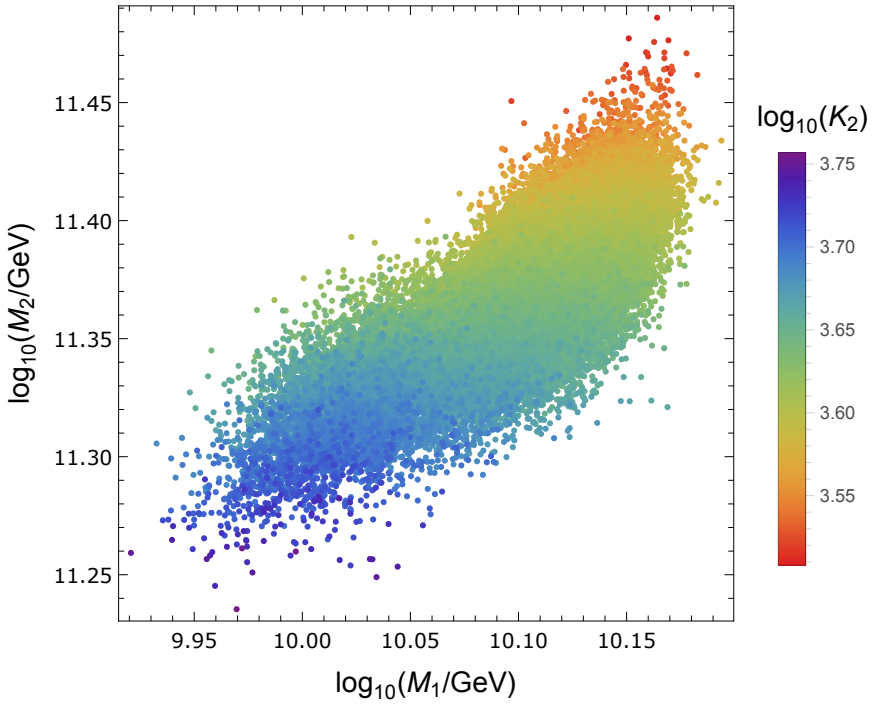

Figure 5.13: Washout in N_R^2 decays.

going to zero matrix.

The three-Yukawa model is more flexible to accommodate low-energy data than the two-Yukawa one, as we parametrize it by 35 free parameters. This enables to fit the model to the low-energy data practically with zero χ^2 with its minimum being likely wider than in the previous case. Given the previous results and the fact that we would definitely get the desired result of successful leptogenesis compatible with flavour fits, we do not repeat the previous analysis.

Nevertheless, as far as we know, no one has dealt with this model yet and we are interested in what influence the perturbation in the form of $\tilde{Y}_{10}$ could have on the characteristics of two-Yukawa model. So instead of scans, we provide the best flavour fit only. In Tab. 5.3, we provide predictions for the best flavour fit of this model corresponding to the following inputs

$$
\begin{aligned}
Y_{10} &= \begin{pmatrix} 2.75\times10^{-6} & 0 & 0 \\ 0 & 6.70\times10^{-6} & 0 \\ 0 & 0 & 0.494 \end{pmatrix}, \\
\tilde{Y}_{10} &= \begin{pmatrix} (-2.65-i2.82)\times10^{-3} & 0.190-i0.269 & 0.244-i0.278 \\ 0.190-i0.269 & -0.422+i0.281 & -1.35+i0.273 \\ 0.244-i0.278 & -1.35+i0.273 & (-1.55+i0.352)\times10^{-6} \end{pmatrix} \\
&\quad \times 10^{-4}, \\
Y_{126} &= \begin{pmatrix} (-1.58+i1.47)\times10^{-8} & (3.25+i3.05)\times10^{-8} & 0.162-i0.320 \\ (3.25+i3.05)\times10^{-8} & -0.733+i1.01 & 0.932-i0.698 \\ 0.162-i0.320 & 0.932-i0.698 & 6.53-i2.45 \end{pmatrix} \\
&\quad \times 10^{-3}, \\
& v_u^{10} = 151\,\text{GeV}, \qquad v_d^{10} = 2.35\,\text{GeV}, \\
& v_u^{126} = (-187+45.6i)\,\text{GeV}, \qquad v_d^{126} = (-18.8-14.6i)\,\text{GeV}, \\
& v_R^{126} = 3.17\times10^{14}\,\text{GeV}, \qquad v_L^{126} = 3.03\times10^{-8}\,\text{GeV}.
\end{aligned}
\tag{5.2}
$$

The value of χ^2 in Tab. 5.3 is computed from pulls according to (4.1), i.e. $\chi^2 \neq 2.98\times10^{-2}$.

In this case, $\tilde{Y}_{10}$ is not negligible, but it is still sub-dominant compared to Y_{10}. It is interesting, that $\tilde{Y}_{10}$ significantly changes some of the parameters, but it leaves the hierarchies intact. Now, Y_{10} has comparable values for the first and second generation and they are smaller by two and three orders, respectively. On the other hand, the third generation changed just a little. Y_{126} still has hierarchical structure and it is still sub-dominant, now it is even much smaller, by two to seven orders. Down-type VEVs are still sub-dominant, but VEVs associated with $\overline{\mathbf{126}}_H$ are amplified at the expense of v_u^{10}. v_R^{126} and v_L^{126} are larger as expected, since they have to compensate smaller Y_{126}.

Regarding the predictions, light neutrino masses are almost unchanged and RHN masses remain hierarchical with lightest RHN mass being smaller by one order. Remarkably enough, η_B is worse than in the two-Yukawa model (cf. Figs. 5.7 and 5.8), but only by two orders, although η_B was not fitted.

Observable	Prediction	Pull/10^{-3}
m_u [MeV]	1.23	-0.975
m_c [GeV]	0.620	1.23
m_t [GeV]	168.3	1.20
m_d [MeV]	2.67	0.750
m_s [MeV]	53.15	-1.81
m_b [GeV]	2.839	-2.41
$\sin\theta_{12}^{\rm CKM}$	0.2251	1.12
$\sin\theta_{13}^{\rm CKM}/10^{-3}$	3.71	-1.02
$\sin\theta_{23}^{\rm CKM}/10^{-2}$	4.180	0.480
$\delta_{\rm CKM}$	1.143	0.798
Δm^2_{21} [10^{-5}eV^2]	7.41	2.02
Δm^2_{31} [10^{-3}eV^2]	2.511	0.717
m_e [MeV]	0.4831	-1.28
m_μ [GeV]	0.1018	2.31
m_τ [GeV]	1.729	-0.571
$\sin^2\theta_{12}^{\rm PMNS}$	0.303	-0.225
$\sin^2\theta_{13}^{\rm PMNS}/10^{-2}$	2.203	0.241
$\sin^2\theta_{23}^{\rm PMNS}$	0.572	0
λ	0.5579	-1.03
χ^2	–	29.8
$\log\eta_B$	-11.74	-8.43
m_1 [meV]	3.70	–
m_2 [meV]	9.37	–
m_3 [meV]	50.2	–
M_1 [GeV]	5.04×10^{9}	–
M_2 [GeV]	4.46×10^{11}	–
M_3 [GeV]	2.22×10^{12}	–
$\delta_{\rm CP}$	1.21	–
ϕ_1	1.12	–
ϕ_2	4.52	–

Table 5.3: Predictions obtained for the best fit of the three-Yukawa model (3.6) with $\chi^2 = 2.98\times10^{-5}$. In addition to the SM observables, several other predictions are also listed.

Conclusion

This thesis provides a comprehensive analysis of leptogenesis in minimal and potentially realistic grand unified models based on non-SUSY SO(10). Leptogenesis as a natural consequence of the seesaw extension of the SM provides and elegant explanation for the baryon asymmetry of the Universe. On the contrary, SO(10) models provide an attractive and more predictive framework for leptogenesis, since it enables quark-lepton unification, it encompasses the seesaw mechanism, and it is able to reproduce experimental measurements. We focus on the Yukawa sector composed of complex scalar representations $\mathbf{10}_H$ and $\overline{\mathbf{126}}_H$, thereby enabling to express the sub-GUT effective field theory in terms of three complex symmetric Yukawa matrices Y_{10}, Y_{126} and $\tilde{Y}_{10}$. By imposing additional global Peccei-Quinn symmetry, one can further reduce the parameter space. We consider both two- and three-Yukawa models with effectively direct symmetry breaking of SO(10) down to the SM and with seesaw mechanism types I and II for generating non-zero light neutrino masses.

We investigate the possibility of successful leptogenesis compatible with flavour fits of these models to updated low-energy data, thereby strictly constraining the parameter space. To this end, we employ the top-down RGE evolution (in order to correctly account for mass thresholds) and evolution of density matrix equations. At the same time, we imitate the seesaw type II as a perturbation of initial condition for effective dimension-five operator and we assume RHN-driven leptogenesis only.

The unique and the most valuable outcomes of our research are parameter scans in the region around the best flavour fit in the two-Yukawa model. Perhaps one of the most striking results of this analysis is that although the fitting procedure was performed independently of the yield of leptogenesis, we get significant set of configurations with the value of BAU within an order of magnitude of the measured value. This remarkable outcome, given the complexity of the problem, provides strong support for the viability of the two-Yukawa SO(10) model. In addition, leptogenesis in this region appears to be dominated by decays of the second lightest RHN as assumed by Mummidi and Patel [33]. However, our study also reveales some limitations. In certain regions of the parameter space, we encountered issues when reproducing η_B on different computers, highlighting the need for more stable methods.

A detailed analysis of the obtained set of configurations reveales several other interesting features. The resulting scan shows preference for hierarchical spectra of RHN masses, aligning with previous studies [29, 33]. However, it prefers heavier N_R^1 compared to [33] considering a similar setup. In the observed region of the parameter space, the scan shows opposing trends in terms of flavour fits and leptogenesis – trend towards lower values of RHN masses in the former case and trend towards larger values in the latter case. The analysis of χ^2 shows dominant pulls from down-quark mass and lepton mixing angles. In particular, it reveales that $\sin^2\theta_{23}^{\mathrm{PMNS}}$ prefers the second local minimum, aligning with [29], while contrasting with [33] that favors the global minimum. This finding highlights the importance of considering the full shape of χ^2 that reflects the experimental measurements.

A surprising finding of our research is obtaining a $B-L$ breaking scale consis-

tent with earlier results [26], although unlike those studies we do not incorporate the unification of running gauge couplings and explicitly solving full RGEs with $B - L$ breaking. This consistency confirms the robustness of the model and suggests that certain key features may be relatively insensitive to the details of the RGE evolution.

Last but not least, we found out that not only Y_{10} is hierarchical, but also Y_{126} prefers a certain hierarchical structure, aligning with best fit parameters reported in [29, 33]. Regarding the VEVs, v_u^{10} is totally dominant and down-type VEVs are sub-dominant as expected from our preliminary discussion.

These results are reproducible in the case of the three-Yukawa model for suppressed $\tilde{Y}_{10}$. The three-Yukawa model is more flexible to accommodate low-energy data and η_B, so the minimum of χ^2 is expected to be wider. Nevertheless, as far as we know, no one has dealt with this model yet. Therefore, we provide its best flavour fit. This shows that perturbation in the form of non-negligible $\tilde{Y}_{10}$ preserves characteristics and some predictions (like light neutrino masses) of the two-Yukawa model. On the other hand, $\tilde{Y}_{10}$ makes Y_{126} smaller and amplifies down-type VEVs at the expense of v_u^{10}. Remarkably, η_B is only about two orders of magnitude worse than in the two-Yukawa model, although η_B was not fitted as in the two-Yukawa model.

In conclusion, this thesis provides results supporting the viability and predictive power of two- and three-Yukawa SO(10) models and robustness of the applied approach. Nevertheless, future research should focus on solving full RGEs incorporating running of Δ_L and more complicated symmetry breaking along with gauge coupling unification. It should focus on leptogensis driven by both RHNs and Δ_L and on numerical stability. It could also explore an even wider regions in the parameter space to potentially uncover other viable regions and/or refine the bounds on model parameters. Investigating the model's implications for other areas of particle physics and cosmology, such as proton decay, could provide further tests of its validity and predictive power. This has to do with the fact that as we continue to push the boundaries of our understanding of the universe, models like those based on SO(10) will play a crucial role for making predictions for upcoming experiments like Hyper-Kamiokande.

Bibliography

[1] S. L. Glashow. Partial Symmetries of Weak Interactions. *Nuclear Physics*, 22(4):579–588, 1961.

[2] S. Weinberg. A Model of Leptons. *Physical Review Letters*, 19(21):1264–1266, 1967.

[3] A. Salam and J. C. Ward. Electromagnetic and weak interactions. *Physics Letters*, 13(2):168–171, 1964.

[4] S. Fukuda et al. Determination of Solar Neutrino Oscillation Parameters using 1496 days of Super-Kamiokande-I Data. *Physics Letters B*, 539(3):179–187, 2002.

[5] B. Aharmim et al. Electron energy spectra, fluxes, and day-night asymmetries of ^{8}B solar neutrinos from measurements with NaCl dissolved in the heavy-water detector at the Sudbury Neutrino Observatory. *Physical Review C*, 72(5):055502, 2005.

[6] S. Abe et al. Precision Measurement of Neutrino Oscillation Parameters with KamLAND. *Phys. Rev. Lett.*, 100(22):221803, 2008.

[7] Planck Collaboration. Planck 2018 results. VI. Cosmological parameters. *arXiv: Cosmology and Nongalactic Astrophysics*, 641:1–67, 2020.

[8] R. L. Workman et al. (Particle Data Group). Review of Particle Physics. *Progress of Theoretical and Experimental Physics*, 2022(8):083C01, 2022.

[9] P. Minkowski. $\mu \to e\gamma$ at a Rate of One Out of 10^9 Muon Decays? *Phys. Lett. B*, 67:421–428, 1977.

[10] T. Yanagida. Horizontal gauge symmetry and masses of neutrinos. *Conf. Proc. C*, 7902131:95–99, 1979.

[11] R. N. Mohapatra and G. Senjanovic. Neutrino Mass and Spontaneous Parity Nonconservation. *Phys. Rev. Lett.*, 44:912, 1980.

[12] J. Schechter and J. W. F. Valle. Neutrino Masses in SU(2) x U(1) Theories. *Phys. Rev. D*, 22:2227, 1980.

[13] M. Fukugita and T. Yanagida. Baryogenesis without grand unification. *Physics Letters B*, 174(1):45–47, 1986.

[14] G. 't Hooft. Symmetry Breaking through Bell-Jackiw Anomalies. *Phys. Rev. Lett.*, 37(1):8–11, 1976.

[15] F. R. Klinkhamer and N. S. Manton. A saddle-point solution in the Weinberg-Salam theory. *Phys. Rev. D*, 30(10):2212–2220, 1984.

[16] V. A. Kuzmin, V. Rubakov, and M. Shaposhnikov. On Anomalous Electroweak Baryon-Number Non-Conservation in the Early Universe. *Physics Letters B*, 155:36–42, 1985.

[17] D. Bödeker and W. Buchmüller. Baryogenesis from the weak scale to the grand unification scale. *Reviews of Modern Physics*, 2021.

[18] M. Magg and C. Wetterich. Neutrino Mass Problem and Gauge Hierarchy. *Phys. Lett. B*, 94:61–64, 1980.

[19] G. Lazarides, Q. Shafi, and C. Wetterich. Proton Lifetime and Fermion Masses in an SO(10) Model. *Nucl. Phys. B*, 181:287–300, 1981.

[20] T. Hambye and G. Senjanovic. Consequences of Triplet Seesaw for Leptogenesis. *Physics Letters B*, 582(1):73–81, 2004.

[21] R. Foot, H. Lew, X. G. He, and G. C. Joshi. See-saw neutrino masses induced by a triplet of leptons. *Zeitschrift für Physik C Particles and Fields*, 44(3):441–444, 1989.

[22] T. et al. Hambye. Constraints on neutrino masses from leptogenesis models. *Nuclear Physics*, 695(1):169–191, 2004.

[23] J. A. Casas and A. Ibarra. Oscillating neutrinos and $\mu \to e, \gamma$. *Nuclear Physics B*, 618(1):171–204, 2001.

[24] H. Georgi and S. L. Glashow. Unity of All Elementary Particle Forces. *Physical Review Letters*, 32(8):438–441, 1974.

[25] P. Langacker. Grand unified theories and proton decay. *Physics Reports*, 72(4):185–385, 1981.

[26] S. Bertolini, L. Di Luzio, and M. Malinský. Intermediate mass scales in the nonsupersymmetric SO(10) grand unification: A reappraisal. *Physical Review D*, 80(1):015013, 2009.

[27] D. Meloni, T. Ohlsson, and S. Riad. Effects of intermediate scales on renormalization group running of fermion observables in an SO(10) model. *Journal of High Energy Physics*, 2014(12):52, 2014.

[28] T. Ohlsson and M. Pernow. Running of Fermion Observables in Non-Supersymmetric SO(10) Models. *Journal of High Energy Physics*, 2018(11):1–16, 2018.

[29] T. Ohlsson and M. Pernow. Fits to Non-Supersymmetric SO(10) Models with Type I and II Seesaw Mechanisms Using Renormalization Group Evolution. *Journal of High Energy Physics*, 2019.

[30] B. Bajc, A. Melfo, G. Senjanovic, and F. Vissani. Yukawa sector in non-supersymmetric renormalizable SO(10). *Physical Review D*, 73(5):055001, 2006.

[31] R. D. Peccei and H. R. Quinn. CP Conservation in the Presence of Pseudoparticles. *Phys. Rev. Lett.*, 38(25):1440–1443, 1977.

[32] K. S. Babu and R. N. Mohapatra. Predictive neutrino spectrum in minimal SO(10) grand unification. *Physical Review Letters*, 70(19):2845–2848, 1993.

[33] V. S. Mummidi and K. M. Patel. Leptogenesis and fermion mass fit in a renormalizable SO(10) model. *Journal of High Energy Physics*, 2021(12):42, 2021.

[34] R. Fonseca, M. Malinský, V. Miřátský, and M. Zdráhal. Leptogenesis in the minimal flipped $SU(5)$ unification, 2023.

[35] P. G. Higgs and P. W. Higgs. Broken Symmetries and the Masses of Gauge Bosons. *Physical Review Letters*, 13(16):508–509, 1964.

[36] P. G. Higgs and P. W. Higgs. Spontaneous Symmetry Breakdown without Massless Bosons. *Physical Review*, 145(4):1156–1163, 1966.

[37] S. Antusch, J. Kersten, M. Lindner, and M. Ratz. Neutrino mass matrix running for non-degenerate see-saw scales. *Physics Letters B*, 538(1):87–95, 2002.

[38] E. W. Otten and Ch. Weinheimer. Neutrino mass limit from tritium β decay. *Reports on Progress in Physics*, 71(8):086201, 2008.

[39] N. Palanque-Delabrouille et al. Neutrino masses and cosmology with Lyman-alpha forest power spectrum. *Journal of Cosmology and Astroparticle Physics*, 2015(11):011–011, 2015.

[40] K. N. Abazajian. Cosmological and Astrophysical Neutrino Mass Measurements. *Astroparticle Physics*, 35(4):177–184, 2011.

[41] A. D. Sakharov. Violation of CP invariance, C asymmetry, and baryon asymmetry of the universe. *Physics-Uspekhi*, 34(5):392–393, 1991.

[42] T. Brauner, O. Taanila, A. Tranberg, and A. Vuorinen. Temperature Dependence of Standard Model CP Violation. *Phys. Rev. Lett.*, 108(4):041601, 2012.

[43] S. Davidson and A. Ibarra. A Lower bound on the right-handed neutrino mass from leptogenesis. *Physics Letters B*, 535(1):25–32, 2002.

[44] A. et al. Granelli. ULYSSES: Universal LeptogeneSiS Equation Solver. *Computer Physics Communications*, 262:107813, 2020.

[45] A. Granelli et al. ULYSSES, universal LeptogeneSiS equation solver: Version 2. *Computer Physics Communications*, 291:108834–108834, 2023.

[46] W. Buchmüller, P. Di Bari, and M. Plümacher. Leptogenesis for pedestrians. *Annals of Physics*, 315(2):305–351, 2005.

[47] L. Doležalová. Effects of a heavy scalar triplet in the primordial lepton asymmetry generation. Master's thesis, Charles University, Prague, 2023.

[48] C. S. Fong, D. Meloni, A. Meroni, and E. Nardi. Leptogenesis in SO(10). *JHEP*, 01:111, 2015.

[49] P. Di Bari and Stephen F. K. Successful N_2 leptogenesis with flavour coupling effects in realistic unified models. *Journal of Cosmology and Astroparticle Physics*, 2015(10):008, 2015.

[50] S. Blanchet, P. Di Bari, D. A. Jones, and L. Marzola. Leptogenesis with heavy neutrino flavours: from density matrix to Boltzmann equations. *Journal of Cosmology and Astroparticle Physics*, 2013(1):041–041, 2013.

[51] F. Hahn-Woernle, M. Plümacher, and Y. Y. Y. Wong. Full Boltzmann equations for leptogenesis including scattering. *Journal of Cosmology and Astroparticle Physics*, 2009(8):028–028, 2009.

[52] G.-y. Huang and S. Zhou. Precise values of running quark and lepton masses in the standard model. *arXiv: High Energy Physics - Phenomenology*, 103(1):016010, 2020.

[53] M. Malinský. *Quark and lepton masses and mixing in supersymmetric grand unified theories*. PhD thesis, SISSA, Trieste, 2005.

[54] R. N. Mohapatra and B. Sakita. SO($2N$) Grand Unification in an SU(N) Basis. *Physical Review D*, 21(4):1062–1066, 1980.

[55] F. del Aguila and L. E. Ibáñez. Higgs bosons in SO(10) and partial unification. *Nuclear Physics*, 177(1):60–86, 1981.

[56] D. Zaharie. A comparative analysis of crossover variants in differential evolution. *Proceedings of the International Multiconference on Computer Science and Information Technology*, pages 171–181, 05 2006.

[57] K. V. Price, R. M. Storn, and J. Lampinen. *Differential Evolution-A Practical Approach to Global Optimization*, volume 141. 01 2005.

[58] T. Deppisch, S. Schacht, and M. Spinrath. Confronting SUSY SO(10) with updated Lattice and Neutrino Data. *Journal of High Energy Physics*, 2019(1):1–25, 2019.

[59] I. et al. Esteban. The fate of hints: updated global analysis of three-flavor neutrino oscillations. *Journal of High Energy Physics*, 2020.

[60] M. A. Acero et al. Improved measurement of neutrino oscillation parameters by the NOvA experiment. *Physical Review D*, 2021.

[61] S. Antusch et al. Running neutrino mass parameters in see saw scenarios. *Journal of High Energy Physics*, 2005.

[62] T. Ohlsson and M. Pernow. Flavor Symmetries in the Yukawa Sector of Non-Supersymmetric SO(10): Numerical Fits Using Renormalization Group Running. *Journal of High Energy Physics*, 2021(9), 2021.

[63] S. Weinberg. Varieties of Baryon and Lepton Nonconservation. *Physical Review D*, 22(7):1694–1700, October 1980.

List of Figures

List of Tables

List of Abbreviations

BAU Baryon Asymmetry of the Universe

BE Boltzmann Equation

BLNV Baryon and Lepton Number Violation

BNV Baryon Number Violation

CKM Cabibbo–Kobayashi–Maskawa

CMB Cosmic Microwave Background

DME Density Matrix Equations

EFT Effective Field Theory

EWPT Electroweak Phase Transition

GUT Grand Unified Theory

LNV Lepton Number Violation

Non-SUSY Non-supersymmetric

OOE Out of Equilibrium

PMNS Pontecorvo-Maki-Nakagawa-Sakata

RGE Renormalization Group Equation

RHN Right-handed Neutrino

SM Standard model

SUSY Supersymmetric

VEV Vacuum Expectation Value

A. Seesaw extension of the Standard Model as an effective field theory

A.1 The effective dimension-five operator

One can understand the SM extensions with the RHNs and/or the scalar triplet as examples of renormalizable models governing the high-energy dynamics and the original SM as a low-energy effective field theory (EFT). In the low-energy regime, the manifestation of such high-energy dynamics can be viewed as d-dimensional effective operators with $d > 4$.

From the scheme of higher-dimensional effective operators of the SM, the lowest-dimensional one that can generate neutrino masses is the dimension-five LNV Weinberg operator [63], cf. [61]:

$$\mathcal{L}_{\text{eff}} = \frac{1}{4}\kappa(\overline{L_L^c}\cdot\Phi)(L_L\cdot\Phi) + \text{h.c.}, \tag{A.1}$$

where $\kappa \equiv -\frac{2}{v^2}M_\nu$.

Type-I and type-II seesaw dynamics can then be viewed through two[1] of the possible renormalizable tree-level 'openings'[2] of the Weinberg operator (A.1).

A.2 Running neutrino masses

The `REAP` package we use for solving RGEs (see Appendix B) incorporates only type-I seesaw mechanism – via Eq. (1.2), in a basis in which M_R is diagonal.

When evolving RGEs from the GUT scale to the M_Z scale, sooner or later the energy scale μ will reach the mass scale M_3. At that scale, the heaviest RHN is integrated out and

$$\kappa \to 2\left(Y_\nu^T\right)_{g3} M_3^{-1}\left(Y_\nu\right)_{3f} \equiv \overset{(3)}{\kappa}_{gf}, \tag{A.2}$$

where we adopted the notation of Ref. [61]. Below M_3, the effective neutrino mass matrix is then given by

$$M_\nu = -\frac{v^2}{2}\left(\overset{(3)}{\kappa} + 2\overset{(3)}{Y}{}_\nu^T \overset{(3)}{M}{}_R^{-1} \overset{(3)}{Y}_\nu\right), \tag{A.3}$$

where $\overset{(3)}{Y}_\nu$ is the 2×3 matrix obtained from Y_ν by removing the last row, and $\overset{(3)}{M}_R$ is the 2×2 matrix obtained from M_R by removing both the last row and the last column.

[1] There is one more possible realisation, related to the propagation of an $\text{SU}(2)_L$ fermion triplet, corresponding to the seesaw type III.

[2] This is similar to the case of the Fermi theory, which can be understood as a low-energy approximation of the SM. In Fermi theory, one can draw a Feynman diagram of the β decay as a direct four-fermion interaction and open it, when going from Fermi theory towards the SM, thereby reconstructing the W boson propagation.

The situation is repeated up to the last threshold M_1. At each threshold, κ is updated as follows:

$$\kappa_{gf} \to \kappa_{gf} + 2\left(Y_\nu^T\right)_{gn} M_n^{-1} \left(Y_\nu\right)_{nf} \equiv \overset{(n)}{\kappa}_{gf}. \tag{A.4}$$

Below M_1, all RHNs are integrated out. We thus get a sequence of sub-GUT EFTs up to the SM. In the whole sequence of EFTs, the effective neutrino mass matrix is thus given by the running of two contributions [61],

$$M_\nu = -\frac{v^2}{2}\left(\overset{(n)}{\kappa} + 2\overset{(n)}{Y}{}_\nu^T \overset{(n)}{M}{}_R^{-1} \overset{(n)}{Y}_\nu\right), \tag{A.5}$$

where n labels the EFTs with $\overset{(2)}{Y}_\nu$ being the 1×3 matrix obtained from Y_ν by removing the last two rows ($\overset{(1)}{M}_R$ is just M_1).

κ in Eq. (A.5) is initially zero. However, by non-zero initial κ, one can imitate type-II seesaw mechanism,

$$\kappa = -\frac{2}{v^2} M_L. \tag{A.6}$$

B. REAP

B.1 Conventions

The `REAP package` contains both one-loop and two-loop RGEs for SM with 3 RHNs (with a few exceptions, which we will come back to). Before we summarize the list of used equations, two remarks are in order here concerning conventions of `REAP`. First, `REAP` uses the RL instead of the LR convention. One can translate between them by transposition (and eventually complex conjugation). However, since Y_{10}, Y_{126} and $\tilde{Y}_{10}$ are symmetric and because of the matching conditions (3.8)–(3.13) and (3.18)–(3.23), the Yukawa matrices are also symmetric.

Second, `REAP` uses the following convention with the unification normalization:

$$g_s = g_3, \quad g = g_2, \quad \sqrt{\frac{5}{3}} g' = g_1. \tag{B.1}$$

B.2 One-loop renormalization group equations

A general form of β function up to two-loop corrections is

$$\overset{(n)}{\beta}_X = \mu \frac{\mathrm{d}\overset{(n)}{X}}{\mathrm{d}\mu} = \overset{(n)}{\beta}{}^{(1)}_X + \overset{(n)}{\beta}{}^{(2)}_X, \tag{B.2}$$

where X is the running parameter and $\overset{(n)}{\beta}{}^{(1)}_X$ and $\overset{(n)}{\beta}{}^{(2)}_X$ are the corresponding one- and two-loop corrections, respectively.

One-loop RGEs for gauge couplings are

$$16\pi^2 \beta^{(1)}_{g_i} = b_i g_i^3, \quad (b_1, b_2, b_3) = \left(\frac{41}{10}, -\frac{19}{6}, -7\right). \tag{B.3}$$

One-loop RGEs for SM Yukawa matrices, Y_ν, M_R, κ, and λ are

$$\begin{aligned}
16\pi^2 \overset{(n)}{\beta}{}^{(1)}_{Y_u} &= Y_u \left[\frac{3}{2} Y_u^\dagger Y_u - \frac{3}{2} Y_d^\dagger Y_d - \frac{17}{20} g_1^2 - \frac{9}{4} g_2^2 - 8 g_3^2 + \right. \\
&\quad \left. + \mathrm{Tr}\left(3 Y_u^\dagger Y_u + 3 Y_d^\dagger Y_d + Y_e^\dagger Y_e + \overset{(n)}{Y}{}^\dagger_\nu \overset{(n)}{Y}_\nu\right)\right], \qquad \text{(B.4)} \\
16\pi^2 \overset{(n)}{\beta}{}^{(1)}_{Y_d} &= Y_d \left[\frac{3}{2} Y_d^\dagger Y_d - \frac{3}{2} Y_u^\dagger Y_u - \frac{1}{4} g_1^2 - \frac{9}{4} g_2^2 - 8 g_3^2 + \right. \\
&\quad \left. + \mathrm{Tr}\left(3 Y_u^\dagger Y_u + 3 Y_d^\dagger Y_d + Y_e^\dagger Y_e + \overset{(n)}{Y}{}^\dagger_\nu \overset{(n)}{Y}_\nu\right)\right], \qquad \text{(B.5)} \\
16\pi^2 \overset{(n)}{\beta}{}^{(1)}_{Y_e} &= Y_e \left[\frac{3}{2} Y_e^\dagger Y_e - \frac{3}{2} \overset{(n)}{Y}{}^\dagger_\nu \overset{(n)}{Y}_\nu - \frac{9}{4} g_1^2 - \frac{9}{4} g_2^2 + \right. \\
&\quad \left. + \mathrm{Tr}\left(3 Y_u^\dagger Y_u + 3 Y_d^\dagger Y_d + Y_e^\dagger Y_e + \overset{(n)}{Y}{}^\dagger_\nu \overset{(n)}{Y}_\nu\right)\right], \qquad \text{(B.6)} \\
16\pi^2 \overset{(n)}{\beta}{}^{(1)}_{Y_\nu} &= \overset{(n)}{Y}_\nu \left[\frac{3}{2} \overset{(n)}{Y}{}^\dagger_\nu \overset{(n)}{Y}_\nu - \frac{3}{2} Y_e^\dagger Y_e - \frac{9}{20} g_1^2 - \frac{9}{4} g_2^2 + \right. \\
&\quad \left. + \mathrm{Tr}\left(3 Y_u^\dagger Y_u + 3 Y_d^\dagger Y_d + Y_e^\dagger Y_e + \overset{(n)}{Y}{}^\dagger_\nu \overset{(n)}{Y}_\nu\right)\right], \qquad \text{(B.7)}
\end{aligned}$$

$$16\pi^2\overset{(n)}{\beta}{}^{(1)}_{\kappa} = \overset{(n)}{\kappa}\left(-\frac{3}{2}Y_e^\dagger Y_e + \frac{1}{2}\overset{(n)}{Y}{}^\dagger_\nu \overset{(n)}{Y}_\nu\right) + \left(-\frac{3}{2}Y_e^\dagger Y_e + \frac{1}{2}\overset{(n)}{Y}{}^\dagger_\nu \overset{(n)}{Y}_\nu\right)^T \overset{(n)}{\kappa} +$$
$$+ \left[2\mathrm{Tr}\left(3Y_u^\dagger Y_u + 3Y_d^\dagger Y_d + Y_e^\dagger Y_e + \overset{(n)}{Y}{}^\dagger_\nu \overset{(n)}{Y}_\nu\right) - 3g_2^2 + \lambda\right]\overset{(n)}{\kappa}, \tag{B.8}$$

$$16\pi^2\overset{(n)}{\beta}{}^{(1)}_{M_R} = \overset{(n)}{Y}_\nu \overset{(n)}{Y}{}^\dagger_\nu \overset{(n)}{M}_R + \overset{(n)}{M}_R \left(\overset{(n)}{Y}_\nu \overset{(n)}{Y}{}^\dagger_\nu\right)^T, \tag{B.9}$$

$$16\pi^2\overset{(n)}{\beta}{}^{(1)}_{\lambda} = 6\lambda^2 - \frac{9}{5}g_1^2\lambda - 9g_2^2\lambda + \frac{27}{50}g_1^4 + \frac{18}{10}g_1^2g_2^2 + \frac{9}{2}g_2^4 + 4\lambda\mathrm{Tr}\left(3Y_u^\dagger Y_u + \right.$$
$$\left. + 3Y_d^\dagger Y_d + Y_e^\dagger Y_e + \overset{(n)}{Y}{}^\dagger_\nu \overset{(n)}{Y}_\nu\right) - 8\mathrm{Tr}\left(3Y_u^\dagger Y_u Y_u^\dagger Y_u + 3Y_d^\dagger Y_d Y_d^\dagger Y_d + \right.$$
$$\left. + Y_e^\dagger Y_e Y_e^\dagger Y_e + \overset{(n)}{Y}{}^\dagger_\nu \overset{(n)}{Y}_\nu \overset{(n)}{Y}{}^\dagger_\nu \overset{(n)}{Y}_\nu\right). \tag{B.10}$$

It is worth recall here that matching relations (3.8)–(3.13) and (3.18)–(3.23) are valid only at the unification scale. We mention it this time because of the property of symmetricity of Yukawa matrices Y_{10}, Y_{126} and $\tilde{Y}_{10}$, which is translated into the symmetricity of matrices Y_u, Y_d, Y_e, Y_ν, M_R, and κ thanks to these relations. However, the cross terms of the type $Y_X Y_Y^\dagger Y_Y$ are symmetry non-conserving, thus Y_u, Y_d, Y_e, and Y_ν do not have to be symmetric below M_{GUT}.

B.3 Two-loop renormalization group equations

Two-loop RGEs for gauge couplings are

$$(4\pi)^4\beta_{g_i}^{(2)} = -\sum_{j=1}^{3}(b_{ji}g_j^2 + c_{ij}T_j)g_i^3, \tag{B.11}$$
$$T = \left(\mathrm{Tr}(Y_uY_u^\dagger), \mathrm{Tr}(Y_dY_d^\dagger), \mathrm{Tr}(Y_eY_e^\dagger)\right),$$
$$b = \begin{pmatrix} -199/50 & -9/10 & -11/10 \\ -27/10 & -35/6 & -9/2 \\ -44/5 & -12 & 26 \end{pmatrix},$$
$$c = \begin{pmatrix} 17/10 & 1/2 & 3/2 \\ 3/2 & 3/2 & 1/2 \\ 2 & 2 & 0 \end{pmatrix}.$$

Two-loop RGEs for SM Yukawa matrices and λ are

$$(4\pi)^4\beta_{Y_u}^{(2)} = Y_u\left[\frac{3}{2}Y_u^\dagger Y_u Y_u^\dagger Y_u - Y_u^\dagger Y_u Y_d^\dagger Y_d - \frac{1}{4}Y_d^\dagger Y_d Y_u^\dagger Y_u + \frac{11}{4}Y_d^\dagger Y_d Y_d^\dagger Y_d + Y_2\cdot\right.$$
$$\cdot\left(\frac{5}{4}Y_d^\dagger Y_d - \frac{9}{4}Y_u^\dagger Y_u\right) - \frac{6}{2}\lambda Y_u^\dagger Y_u + \left(\frac{223}{80}g_1^2 + \frac{135}{16}g_2^2 + 16g_3^2\right)Y_u^\dagger Y_u -$$
$$- \left(\frac{43}{80}g_1^2 - \frac{9}{16}g_2^2 + 16g_3^2\right)Y_d^\dagger Y_d - \chi_4 + \frac{3}{8}\lambda^2 + \frac{5}{2}Y_4 + \left(\frac{9}{200} + \frac{29}{45}n_g\right)\cdot$$
$$\cdot\, g_1^4 - \frac{9}{20}g_1^2g_2^2 + \frac{19}{15}g_1^2g_3^2 - \left(\frac{35}{4} - n_g\right)g_2^4 + 9g_2^2g_3^2 -$$
$$\left. - \left(\frac{404}{3} - \frac{80}{9}n_g\right)g_3^4\right] \tag{B.12}$$

$$
\begin{aligned}
(4\pi)^4\beta_{Y_d}^{(2)} = {} & Y_d\left[\frac{3}{2}Y_d^\dagger Y_d Y_d^\dagger Y_d - Y_d^\dagger Y_d Y_u^\dagger Y_u - \frac{1}{4}Y_u^\dagger Y_u Y_d^\dagger Y_d + \frac{11}{4}Y_u^\dagger Y_u Y_u^\dagger Y_u + Y_2\cdot\right. \\
& \cdot\left(\frac{5}{4}Y_u^\dagger Y_u - \frac{9}{4}Y_d^\dagger Y_d\right) - \frac{6}{2}\lambda Y_d^\dagger Y_d + \left(\frac{187}{80}g_1^2 + \frac{135}{16}g_2^2 + 16g_3^2\right)Y_d^\dagger Y_d - \\
& - \left(\frac{79}{80}g_1^2 - \frac{9}{16}g_2^2 + 16g_3^2\right)Y_u^\dagger Y_u - \chi_4 + \frac{3}{8}\lambda^2 + \frac{5}{2}Y_4 - \left(\frac{29}{200} + \frac{1}{45}n_g\right)\cdot \\
& \cdot g_1^4 - \frac{27}{20}g_1^2 g_2^2 + \frac{31}{15}g_1^2 g_3^2 - \left(\frac{35}{4} - n_g\right)g_2^4 + 9g_2^2 g_3^2 - \\
& \left. - \left(\frac{404}{3} - \frac{80}{9}n_g\right)g_3^4\right] \qquad \text{(B.13)} \\
(4\pi)^4\beta_{Y_e}^{(2)} = {} & Y_e\left[\frac{3}{2}Y_e^\dagger Y_e Y_e^\dagger Y_e - \frac{9}{4}Y_2 Y_e^\dagger Y_e - \frac{6}{2}\lambda Y_e^\dagger Y_e + \left(\frac{387}{80}g_1^2 + \frac{135}{16}g_2^2\right)Y_e^\dagger Y_e - \right. \\
& - \chi_4 + \frac{3}{8}\lambda^2 + \frac{5}{2}Y_4 + \left(\frac{51}{200} + \frac{11}{5}n_g\right)g_1^4 + \frac{27}{20}g_1^2 g_2^2 - \\
& \left. - \left(\frac{35}{4} - n_g\right)g_2^2\right] \qquad \text{(B.14)} \\
(4\pi)^4\beta_{\lambda}^{(2)} = {} & 2\left\{-\frac{78}{8}\lambda^3 + \left(54g_2^2 + \frac{54}{5}g_1^2\right)\frac{\lambda^2}{4} - \left[\left(\frac{313}{8} - 10n_g\right)g_2^4 - \frac{117}{20}g_2^2 g_1^2 - \right.\right. \\
& \left. - \left(\frac{687}{200} + 2n_g\right)g_1^4\right]\frac{\lambda}{2} + \left(\frac{497}{8} - 8n_g\right)g_2^6 - \left(\frac{97}{40} + \frac{8}{5}n_g\right)g_2^4 g_1^2 - \\
& - \left(\frac{717}{200} + \frac{8}{5}n_g\right)g_2^2 g_1^4 - \left(\frac{531}{1000} + \frac{24}{25}n_g\right)g_1^6 - 64g_3^2\mathrm{Tr}\left(Y_u^\dagger Y_u Y_u^\dagger Y_u + \right. \\
& \left. + Y_d^\dagger Y_d Y_d^\dagger Y_d\right) - \frac{8}{5}g_1^2\mathrm{Tr}\left(2Y_u^\dagger Y_u Y_u^\dagger Y_u - Y_d^\dagger Y_d Y_d^\dagger Y_d + 3Y_e^\dagger Y_e Y_e^\dagger Y_e\right) - \\
& - \frac{3}{2}g_2^4 Y_2 + g_1^2\left[\left(\frac{63}{5}g_2^2 - \frac{171}{50}g_1^2\right)\mathrm{Tr}\left(Y_u^\dagger Y_u\right) + \left(\frac{27}{5}g_2^2 + \frac{9}{10}g_1^2\right)\cdot\right. \\
& \left.\cdot\mathrm{Tr}\left(Y_d^\dagger Y_d\right) + \left(\frac{33}{5}g_2^2 - \frac{9}{2}g_1^2\right)\mathrm{Tr}\left(Y_e^\dagger Y_e\right)\right] + 5\lambda Y_4 - 6\lambda^2 Y_2 - \frac{\lambda}{2}H - \\
& - 21\lambda\mathrm{Tr}(Y_u^\dagger Y_u Y_d^\dagger Y_d) + 20\mathrm{Tr}\left(3Y_u^\dagger Y_u Y_u^\dagger Y_u Y_u^\dagger Y_u + 3Y_d^\dagger Y_d Y_d^\dagger Y_d Y_d^\dagger Y_d + \right. \\
& \left.\left. + Y_e^\dagger Y_e Y_e^\dagger Y_e Y_e^\dagger Y_e\right) - 12\mathrm{Tr}\left[Y_u^\dagger Y_u\left(Y_u^\dagger Y_u + Y_d^\dagger Y_d\right)Y_d^\dagger Y_d\right]\right\}, \qquad \text{(B.15)}
\end{aligned}
$$

where

$$
\begin{aligned}
n_g &= 3, && \text{(B.16)} \\
Y_2 &= \mathrm{Tr}\left(3Y_u^\dagger Y_u + 3Y_d^\dagger Y_d + Y_e^\dagger Y_e\right), && \text{(B.17)} \\
H &= \mathrm{Tr}\left(3Y_u^\dagger Y_u Y_u^\dagger Y_u + 3Y_d^\dagger Y_d Y_d^\dagger Y_d + Y_e^\dagger Y_e Y_e^\dagger Y_e\right), && \text{(B.18)} \\
Y_4 &= \left(\frac{17}{20}g_1^2 + \frac{9}{4}g_2^2 + 8g_3^2\right)\mathrm{Tr}\left(Y_u^\dagger Y_u\right) + \left(\frac{1}{4}g_1^2 + \frac{9}{4}g_2^2 + 8g_3^2\right)\mathrm{Tr}\left(Y_d^\dagger Y_d\right) + \\
&\quad + \frac{3}{4}(g_1^2 + g_2^2)\mathrm{Tr}\left(Y_e^\dagger Y_e\right), && \text{(B.19)} \\
\chi_4 &= \frac{9}{4}\mathrm{Tr}\left(3Y_u^\dagger Y_u Y_u^\dagger Y_u + 3Y_d^\dagger Y_d Y_d^\dagger Y_d + Y_e^\dagger Y_e Y_e^\dagger Y_e - \frac{1}{3}Y_u^\dagger Y_u Y_d^\dagger Y_d + \right. \\
&\quad \left. + Y_d^\dagger Y_d Y_u^\dagger Y_u\right). && \text{(B.20)}
\end{aligned}
$$

Two-loop RGEs of Y_ν, M_R and κ are not implemented in `REAP` package yet. Nevertheless, they have a mild running already at one-loop level.